EFFECTS OF ELECTRICAL FIELD ON THE IMMUNOLOGICAL PROPERTIES OF PARATHYROID CELLS

by
Saime Bengü Kaptanoğlu

Submitted to Graduate School of Natural and Applied Sciences
in Partial Fulfilment of the Requirements
for the Degree of Master of Science in
Biotechnology

Yeditepe University
2023

EFFECTS OF ELECTRICAL FIELD ON THE IMMUNOLOGICAL PROPERTIES OF PARATHYROID CELLS

APPROVED BY:

Prof. Dr. Mustafa Erhan Ayşan .....
(Thesis Supervisor)
(Yeditepe University)

Assist. Prof. Dr. Özge Acar .....
(Thesis Co- supervisor)
(Istanbul Okan University)

Prof. Dr. Fikrettin Şahin .....
(Yeditepe University)

Prof. Dr. Gamze Torun Köse .....
(Yeditepe University)

Assist. Prof. Dr. Harun Başoğlu .....
(Karadeniz Technical University)

DATE OF APPROVAL: ..../..../2023

I hereby declare that this thesis is my work and that all information in this thesis has been obtained and presented by academic rules and ethical conduct. I have fully cited and referenced all material and results as required by these rules and conduct and this thesis study does not contain any plagiarism. The necessary permissions have been obtained if any material used in the thesis requires copyright. No material from this thesis has been used for the award of another degree.

I accept all kinds of legal liability that may arise in cases contrary to these situations.

Name, Last name Saime Bengü Kaptanoğlu

Signature …..……..……..

ACKNOWLEDGEMENTS

Firstly, I would like to thank my supervisors, Prof. Dr. Erhan Ayşan, co- supervisor Assist. Prof. Dr. Özge Acar, and advisor Prof. Dr. Gamze Torun Köse for their guidance and assistance.

Gratias tibi omnes pro hoc omnia tolerabilia. I would like to express my deepest gratitude to my teammates, Ahmed Alperen Tuncer, Gülnihal Bozdağ, and Gülçin Delal Nozhatzadeh, who have always been there for me inside, and outside the workplace. I cannot think of any other group of people better to work with.

I would like to thank all my friends, Buse Bayrakci, Batuhan Turan Bozkurt, Gülşah Şebnem Özköse, and Ece Tezsezen, who tolerated me over during stressful times and helped me when I needed to hear the good and the bad.

Lastly, I would like to thank my family, my parents Aysan Susmuş Kaptanoğlu and Koray Kaptanoğlu. I would also like to pay my respects to my late grandmother Nevin Kaptanoğlu. She had always inspired me in everything I did, especially ever since she started telling me stories about her time in the biology department at Istanbul University. I would like to dedicate this thesis to her, hoping she is as proud as I am.

ABSTRACT

EFFECTS OF ELECTRICAL FIELD ON THE IMMUNOLOGICAL PROPERTIES OF PARATHYROID CELLS

The only unique and permanent treatment option for hypoparathyroidism is the allotransplantation of the parathyroid (Pt) gland or Pt cells. Immunosuppressive medication regimens are required after transplantation to prevent the host's immune system from rejecting the transplant. However, these medications might not be required if the transplanted cells do not express any immunological markers, such as human leukocyte antigen (HLA) surface proteins, that would be recognized by the host immune system. Additionally, electric fields (EFs) are well recognized as an outside factor that can influence gene expression, cellular morphology, differentiation potential, and proliferation. The purpose of this study is to increase allotransplantation success rates by reducing or completely eliminating HLA expression or causing it to have non-functional forms by exposing cells to controlled EFs without affecting their viability or function. Human dermal fibroblast (HDF) and Pt cells were cultured between two aluminium plates and subjected to EFs between 0, 600, and 1200 volts (V) for 1 hour (h). Cell viability was measured using flow cytometry, and the effects on the expression of various HLA proteins were measured using polymerase chain reaction (PCR). The expressions of HLA-A (0.35 ± 0.14- fold change, $p<0.001$) and HLA- C (0.60 ± 0.04-fold change, $p<0.0001$) were significantly decreased in HDF cells exposed to a 1200 V EF without any significant changes to their viability. On the other hand, HLA- A (0.47 ± 0.16- fold change, $p<0.01$) and HLA- B (0.35 ± 0.122- fold change, $p<0.001$) levels decreased significantly in Pt cells exposed to 1200 V EF. PTH expression increased significantly (1.46 ± 0.29- fold change, $p<0.05$) after 1200 V EF exposure. PTH secretion increased 20 h after EF application in both 600 V (1689.3 pg/mL ± 392.1, $p<0.0001$) and 1200 V (1329.0 ± 167.39 pg/mL, $p<0.001$). The impact of the EF on the gene expression of HDF and Pt cells varied by voltage. The EF application did not alter the viability of either of the cell lines. These findings suggest that with a possible decreased level of HLA class I gene expression, the requirement for immunosuppressants upon Pt transplantation might decrease. Thus, these results suggest a promising new procedure for Pt transplantation.

ÖZET

ELEKTRİK ALANININ PARATİROİD HÜCRELERİN İMMÜNOLOJİK ÖZELLİKLERİ ÜZERİNDEKİ ETKİLERİ

Hipoparatiroidizm için tek benzersiz ve kalıcı tedavi seçeneği, paratiroid (Pt) bezinin veya Pt hücrelerinin allotransplantasyonudur. Hastanın bağışıklık sisteminin nakli reddetmesini önlemek için nakilden sonra immünsüpresif ilaçlar gerekmektedir. Bununla birlikte, nakledilen hücreler, hastanın bağışıklık sistemi tarafından tanınabilecek insan lökosit antijeni (HLA) yüzey proteinleri gibi herhangi bir immünolojik belirteç ifade etmiyorsa bu ilaçlar gerekli olmayabilir. Ek olarak, elektrik alanın (EF) gen ekspresyonunu, hücresel morfolojiyi, farklılaşma potansiyelini ve proliferasyonu etkileyebilecek bir dış faktör olduğu iyi bilinmektedir. Bu çalışmanın amacı, kontrollü EF uygulaması yoluyla hücrelerin canlılığını ve fonksiyonlarını etkilemeden HLA ekspresyonunu azaltarak veya kaldırarak veya fonksiyonel olmayan formlarını oluşturarak allotransplantasyon başarı oranlarını arttırmaktır. İnsan dermal fibroblast hücreleri (HDF) ve Pt hücreleri, 1 saat boyunca 0, 600 ve 1200 volt (V) elektrik alan uygulanarak iki alüminyum plaka arasında kültürlendi. Hücre canlılığı, akış sitometrisi kullanılarak ölçüldü ve çeşitli HLA gen ekspresyonları üzerindeki etkileri, polimeraz zincir reaksiyonu (PCR) kullanılarak ölçüldü. HLA- A (0,35 ± 0,14 kat değişiklik, $p<0,001$) ve HLA- C (0,60 ± 0,04 kat değişiklik, $p<0,0001$) ifadeleri, 1200 V EF'ye maruz bırakılan HDF hücrelerinin canlılığında anlamlı bir değişiklik olmaksızın önemli ölçüde azaldı. Öte yandan, 1200 V EF'ye maruz bırakılan Pt hücrelerinde HLA- A (0,47 ± 0,16 kat değişiklik $p<0,001$) ve HLA- B (0,35 ± 0,122 kat değişiklik $p<0,0001$) önemli ölçüde azalırken, PTH ekspresyonu, 1200 V EF maruziyetinden sonra önemli ölçüde arttı (1,46 ± 0,29 kat değişiklik $p<0,05$). PTH salgılanmasının, hem 600 V (1689,3 pg/mL ± 392,1 $p<0,0001$) hem de 1200 V'ta (1329,0 ± 167,39 pg/mL $p<0,001$) EF uygulamasından 20 saat sonra arttığı gözlemlendi. Voltaj kaynağının gücüne bağlı olarak, EF'nin HDF ve Pt hücrelerinin gen ekspresyonu üzerindeki etkisi değişiklik göstermiştir. Her iki hücre tipine EF uygulaması, bu hücrelerin canlılığını değiştirmedi. Bu bulgular, olası bir azalmış HLA sınıf I gen ekspresyonu seviyesi ile, Pt transplantasyonu için kullanılan immünosupresanlara olan ihtiyacın azalabileceğini göstermektedir. Bu nedenle, bu sonuçlar Pt nakli için umut verici yeni bir prosedür önermektedir.

TABLE OF CONTENTS

LIST OF FIGURES

LIST OF TABLES

LIST OF SYMBOLS/ABBREVIATIONS

APC	Antigen presenting cell
BSA	Bovine serum albumin
CaSR	Calcium sensing receptor
CD94/NKG2	Killer cell lectin- like receptor subfamily C
CLIP	Class II- associated invariant chain peptide
cm	Centimetre
CTLA- 4	Cytotoxic T- lymphocyte associated protein 4
DC	Dendritic cell
DMEM HG	Dulbecco’s modified eagle media high glucose
DMSO	Dimethyl sulfoxide
DNA	Deoxyribonucleic acid
DNase	Deoxyribonuclease
DNMT1	DNA methyltransferase 1
DPBS	Dulbecco’s phosphate buffered saline
EDTA	Ethylenediamine tetraacetic acid
EF	Electric field
ELF- EMF	Extremely low frequency electromagnetic field
ELISA	Enzyme- linked immunoassay
EMF	Electromagnetic field
ER	Endoplasmic reticulum
ERAP1	Endoplasmic reticulum aminopeptidase 1
ERAP2	Endoplasmic reticulum aminopeptidase 2
ERK	Extracellular signal- regulated kinase
ERp57	Endoplasmic reticulum protein 57
FBS	Fetal bovine serum
GAPDH	Glyceraldehyde- 3- phosphate dehydrogenase
GCM2	Glial cells missing 2
GHz	Gigahertz
Gy	Gray
h	Hour
HDF	Human dermal fibroblast

HLA	Human leukocyte antigen
HyperPT	Hyperparathyroidism
HypoPT	Hypoparathyroidism
IFN- γ	Interferon- γ
Ig	Immunoglobulin
Ii	Invariant chain
IL- 2	Interleukin- 2
IL- 2R	IL- 2 receptor
ILT- 2	Ig- like transcript- 2
ILT- 4	Ig- like transcript- 4
ITS	Insulin- transferrin- selenium.
kHz	Kilohertz
KIR	Killer Ig- like receptor
KIR2DL4	Killer cell immunoglobulin like receptor, two Ig domains and long cytoplasmic tail 4
kV/cm	Kilovolts / centimetre
LNSC	Lymph node stromal cell
m	metre
MCR5	Human lung fibroblast cell line
MDB	Membrane desalting buffer
MHC	Major histocompatibility complex
MICA	MHC class I chain- related A
MICB	MHC class I chain- related B
MIIC	MHC Class II- e- enriched compartment
min	Minute
mm	Millimetre
mRNA	Messenger RNA
mV/mm	Millivolts /millimetre
MV/mm	Megavolts / millimetre
MV/m	Megavolts / meter
NK	Natural killer
nsPEF	Nanosecond PEF
PBS	Phosphate buffered saline

PCR	Polymerase chain reaction
PEF	Pulsed EF
PI3K	Phosphatidylinositol- 3 kinase
PS	Penicillin streptomycin
Pt	Parathyroid
PTH	Parathormone
PTH1R	PTH receptor 1
qPCR	Quantitative polymerase chain reaction
RLN	Recurrent laryngeal nerve
RNA	Ribonucleic acid
RPMI 1600	Roswell park memorial institute media 1600
ROS	Reactive oxygen species
RT- PCR	Reverse- transcription PCR
sec	Second
SEF	Static EF
SPPase	Signal peptide peptidase
TAP	Transporter associated with antigen processing
TBE	Tris- borate EDTA
TCR	T cell receptor
Th1	T helper 1
TNF- α	Tumour necrosis factor- α
V	Volt
V/cm	Volts / centimetre
v/v	Volume / volume
VEGFR	Vascular endothelial growth factor receptor
βm2	β2 microglobul

1. INTRODUCTION

1.1. PARATHYROID

The parathyroid (Pt) is an endocrine organ that normally weighs 40–60 mg and measures around 2 mm x 4 mm x 6 mm. While it is generally found in four pieces, this number may vary in some rare cases [1–4]. At the early stages of development, the glands have a half-transparent, grayish color. As the newborn gets older, the color changes from gray to a golden yellow, followed by a yellowish brown. The color could relate to the amount of fat tissue within the gland [3].

Despite the fact that the Pt, thymus, and thyroid all share the same precursors in early fetal development, the Pt functions more like the thyroid than the thymus [5,6]. A fetus develops four branchial clefts and five branchial pouches in the fifth to sixth week of pregnancy, which originate from the ectoderm and endoderm, respectively [7]. Dorsal epithelial thickens from the third and fourth branchial pouches, developing into the Pt, thymus, and thyroid glands [8]. There are two sets of Pt glands, the superior and the inferior, which originate from different branchial pouch (Figure 1.1). The superior Pt and thyroid glands originate from the fourth branchial pouch [1]. Superior Pt glands are generally located on the upper or middle section of the thyroid gland; however, they have been observed in the paraoesophageal or retroesophageal sections in some cases [2,9,10]. In some cases, superior Pt glands could be seen on the underside of inferior Pt glands [10]. The rarest location anomaly of the superior Pt gland is called ectopic superior Pt, which refers to the abnormally localized superior Pt in the middle or posterior mediastinum or aortopulmonary window [2]. In contrast, inferior Pt glands arise from third branchial pouches with the thymus. The normal localization of inferior Pt glands is within 1 cm of the junction between the inferior thyroid artery and the recurrent laryngeal nerve (RLN). In the case of inferior Pt glands, localization abnormalities are a more common occurrence since, during embryonic development, they migrate caudally in the neck [1]. Around 15 – 50% of inferior Pt glands are localized at the thymus [2,11]. In the case of undescended inferior PT glands, several different localizations are observed, such as around the skull base, intrathyroidal glands, and at the angle of the mandible. They could also be found in the upper part of the superior Pt glands [12].

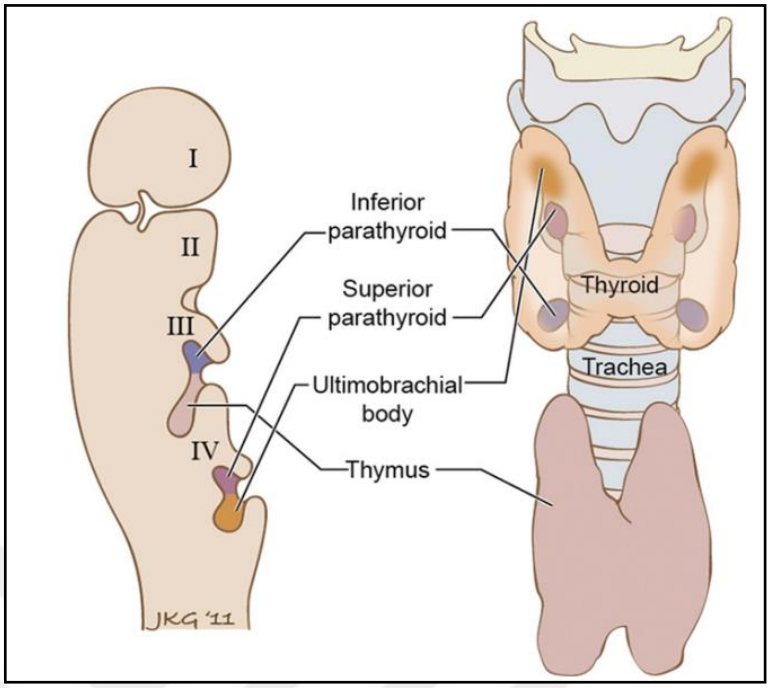

Figure 1. 1. Localization of Thyroid, Pt, and Thymus in Anatomic and Early Developmental States [13].

The Pt is a gland that is known to be responsible for the secretion of parathormone (PTH). Calcium- phosphate homeostasis is dependent on PTH secretion from Pt cells [6]. There are two types of cells in the gland: chief cells and oxyphil cells. PTH is secreted from chief cells after stimulation of the calcium- sensing receptor (CaSR) when blood calcium levels are low [14]. While chief cells and oxyphil cells have certain similarities, it is not yet known whether oxyphil cells can secrete or control the release of PTH in a manner similar to chief cells [15]. Chief cells make up the majority of the Pt gland's cell population when a person is young, but as they get older, oxyphil cells take over [16]. The oxyphil cells are larger than the chief cells and have more acidophilic cytoplasm than the chief cells, caused by their mitochondrial activity. Observations of acidophilic cytoplasms with sizes similar to those of chief cells suggest that oxyphil cells derive from chief cells [17]. This idea of trans- differentiation is also supported by the expression of PTH in oxyphil cells [15] and the lack of glial cells missing 2 (GCM2) expression, which is a transcription factor essential for Pt gland development [18].

PTH is composed of 84 amino acids that form a single- chain protein structure. PTH is cleaved from the pre- pro- PTH beforehand and stored in the granules, waiting for either

degradation or secretion. PTH production in Pt closely depends on extracellular calcium levels. In cases of hypercalcemia, the synthesis of PTH is reduced; however, fragments of PTH may still be secreted [19]. The classical PTH working mechanism reduces phosphate reabsorption by the kidney [20–22] and increases blood calcium levels [23] through calcium trimming from bone tissue [24–26], formation of active vitamin D compounds [27,28], and renal calcium resorption [29].

Since the calcium-phosphate metabolism cannot be controlled without affecting both the absorption and elimination of these ions, PTH secretion affects several different organs. Thus, PTH receptor 1 (PTH1R) is found on the surface of a variety of cell types in a wide range of tissues, including kidneys and bones. PTH1R is a transmembrane protein that, when activated by PTH, activates several pathways, including Protein Kinase A and C. The intracellular mechanisms that are stimulated through PTH depend on the cell type [30].

Hyperparathyroidism (HyperPT) is an endocrine disorder, which is caused by an excessive amount of PTH secretion and hypercalcemia. Patients with hyperphosphatemia have some common symptoms, including hypercalcemia and hypophosphatemia [30]. There are three classifications for HyperPT: primary, secondary, and tertiary. The over- secretion of PTH in the primary type could be a result of a Pt adenoma. In rare cases, hyperplasia or carcinoma may occur [31]. The common symptoms of primary HyperPT are increased urination, thirst, kidney stones, depression, and fatigue [32]. On the other hand, secondary hyperphosphatemia is caused by other problems, such as renal failure, vitamin D deficiency, or gastrointestinal malfunction, which then result in high blood calcium levels. Researchers have multiple theories for what causes secondary HyperPT. Chronic renal failure is diagnosed by excessive calcium and decreased phosphate levels, yet in malabsorption and vitamin D deficiency cases, low phosphate and low vitamin D are observed, as well as high blood calcium [32]. The most common treatment for primary and secondary HyperPT is parathyroidectomy [34]. Lastly, tertiary HyperPT is a rare disorder; however, it is possible to observe this condition in cases of elevated secretion of PTH, most often after renal transplantation [30,32].

Another endocrine disorder caused by insufficient PTH secretion is hypoparathyroidism (HypoPT). Even though hypoparathyroidism is not as common as hyperparathyroidism, it could be caused by a thyroid resection and damage to the gland during surgery. Autoimmune disorders, which disrupt either the hormone itself or the integrity of the gland individually

or collectively, are another common cause of insufficient PTH secretion [35,36]. In the autoimmune polyendocrine syndrome type, a mutation in the autoimmune regulatory gene causes hypophosphatemia as well as other disorders such as Addison disease [36]. On the other hand, in the case of DiGeorge syndrome, HypoPT is a result of a chromosomal deletion in 22q11. Due to this deletion, the embryonic development of the thymus and Pt glands is disrupted [35].

Hypocalcemia, which causes muscle cramps, paranesthesia, and abdominal pain, can be used to diagnose HypoPT. Hypocalcemia and hyperphosphatasemia are thought to be the causes of these symptoms. Even though there are treatments for HypoPT symptoms, such as recombinant PTH treatment, vitamin D, and calcium supplements, they do not provide a permanent cure for the disorder. Pt transplantation is a unique and permanent treatment option for HypoPT with a lower cost [37–39].

Pt transplantation is an effective treatment for hypoparathyroidism caused by autoimmune dysfunction or damage after thyroidectomy [39]. The transplantation protocol could differ according to the characteristics of the transplant; the tissue could be transplanted as a whole or in smaller pieces, or after isolating Pt cells, those cells could be transplanted. The risk of a negative immunological response cannot be avoided because allotransplantation is the only option available to the majority of HypoPT patients. Just as in every other transplantation protocol, the host's immune system is kept under control with the use of immunosuppressants. Despite increasing the likelihood of transplant survival, immunosuppressant drugs may also decrease patients' natural defense mechanisms, making them susceptible to pathogens or tumor formation [41,42]. In the case of Pt transplantation, different immunosuppressants are used before and after the protocol. Additional strategies are used to increase the likelihood of a successful transplant, such as the encapsulation of the tissue or cells within natural and/or biocompatible materials. These methods increase the survival rates for the transplant and/or reduce the recipient's dependence on immunosuppressive drugs. Such biocompatible materials include sodium alginate [43], chitosan [43], collagen [44], cellulose [45], and agarose [46].

Sodium alginate is a natural biocompatible material that is generally used in Pt allotransplantations as a barrier between the transplant and the recipient. In a case report published in 2019, Pt cells were mechanically isolated and encapsulated with sodium alginate. The microcapsules were transplanted into the omental tissue of a 37-year-old

female by our group. Even though the patient required immunosuppressant treatment after the surgery, one- year follow- up reports proved that the recipient did not require any other medication based on her HypoPT [47].

1.2. TRANSPLANTATION IMMUNOLOGY

Transplantation immunology is an area that is focused on the immune reactions that occur in the transplant recipient against the allograft. Alloreaction is the concept of the immune system's reaction to a graft or a tissue even though the source of the tissue is from the same species as the host. It is generally caused by cell-mediated immune reactions, with the key players in this action being the T lymphocytes [49,50]. Even though other innate immune cells such as macrophages and natural killer (NK) cells also have alloreactive responses, most of the damage done to the graft is caused by T lymphocytes [51]. Alloreaction is distinguished by the fact that the precursor frequency of alloreactive T lymphocytes is 100 to 1000 times higher than that of any other non- self- antigen- specific T lymphocyte [52]. The high precursor frequency of alloreactive T cells (up to 10^4) allows them to be easily detected during a primary immune response [52,53]. There are two hypotheses for the alloreactive T cell interactions with the allogeneic major histocompatibility complex (MHC). A comprehensive model of alloreactive T cell recognition is based on the interaction of allogenic MHC and the T cell receptor (TCR) (Figure 1.2) [54]. The other theory suggests that the presented peptide has a crucial role in the alloreactivity of T lymphocytes [55]. Even though researchers try to differentiate conventional TCR-MHC interaction from alloreactive activation, findings showed that alloreactive activation and conventional activation through MHC- TCR interaction are not distinct. Furthermore, several studies [55–57] found highly peptide- specific alloreactive T lymphocytes.

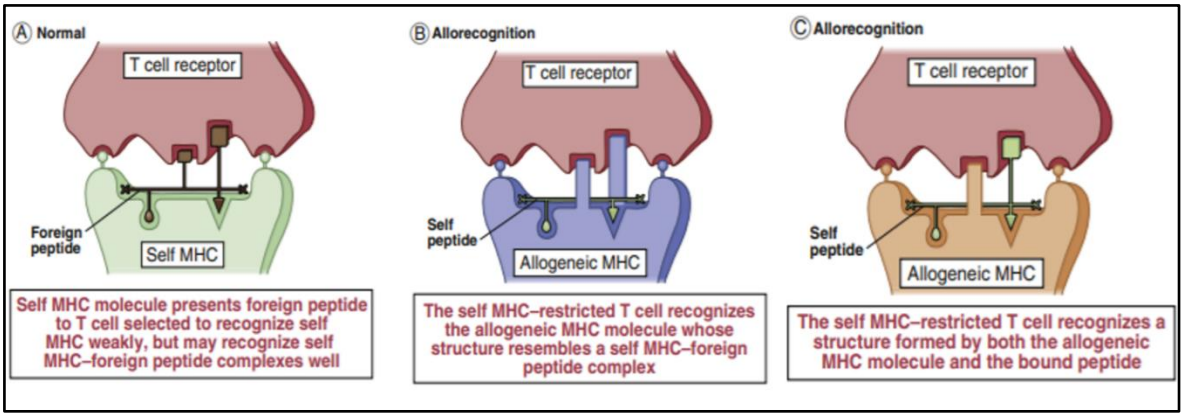

Figure 1. 2. Comparison of conventional (A) and the two theoretical models of T cell activation (B, C) [58].

Another major reason for transplant failure is donor human leukocyte antigen (HLA)-mediated immune responses [57]. Donor- specific antibodies are assumed to be the cause of chronic antibody- mediated rejection. Interactions between donor HLA- specific $CD4^+$ T lymphocytes and B lymphocytes induce the production of donor HLA- specific antibodies [58,59]. However, B lymphocyte actions could also cause operational tolerance to allogenic antigens [62–67].

There are several potential reactions by the host's immune system to the transplant. Different responses affect the patient at different rates. To begin, in a hyperacute reaction, donors' specific antibodies bind to blood vessel endothelial cells and activate the complement system, causing endothelial cells to be damaged and releasing surface heparin sulfate. Endothelial cells secrete a high- molecular- weight protein called the Von Willebrand factor into the surrounding microenvironment [66]. This factor promotes thrombosis and platelet clumping. Even if the transplant survives this response, it delays vascular rejection attacks for 36 48 h [56]. Since NK cells regulate vascular rejection via the interaction of the NK cell's fragment crystallizable receptor with cell- bound immunoglobulin G, this is known as a type of antibody- mediated cellular cytotoxicity [67]. Increased damage to the tissue leads to more vascular thrombosis. The hyperacute reaction is rare since the recipients are scanned for any possible antibody match to the donor tissue [56]. The acute reaction starts showing symptoms after the first week of transplantation. Dendritic cells (DC) from the donor's tissue directly or indirectly activate alloreactive T lymphocytes. $CD8^+$ T lymphocytes are activated when donor DCs migrate to the lymph node and express non- self HLA and other co-

stimulatory molecules [68]. This migration initiates a chain reaction of alloreaction that directs cytotoxic T cells to the endothelial cell population of the graft. In addition, $CD4^+$ T helper 1 (Th1) cells are activated, and inflammatory cytokines are released to control innate and adaptive immune cell migration to the graft microenvironment. These immune responses to the transplant cause vascular endothelin or intimal arteritis, which could lead to graft damage [56,69]. Chronic graft rejection, which includes both cell- mediated and antibody-mediated immune reactions, may be observed in the recipient six months to one year after transplantation. Almost every transplantation process has a different rejection pathway, especially chronic rejection, which could be defined by different scenarios based on graft type. Chronic rejection, for example, causes vanishing bile duct syndrome in liver transplants [70], tissue damage and blood vessel scarring in kidney transplants [71], and coronary vessel narrowing in chronic cardiac rejection [72].

1.2.1. Major Histocompatibility Complex

The journey to the discovery of one of the most important immunobiological complexes started with research on tumor biology in the early 1900s. Snell dubbed the resistance genes he discovered as histocompatibility genes, or H genes. Gorer and Snell together discovered that antigen II is a protein structure that is encoded in the H genes. This locus was later dubbed the histocompatibility- 2 (H- 2) locus [73]. Snell and his colleagues focused on H- 2 in the years that followed, discovering various antigens encoded in the locus [76]. In 1980, Snell was awarded the Nobel Prize for his and Gorer's discoveries about histocompatibility. After the discovery of other H- 2 loci, the H- 2 locus started being called the H complex, and later on, the name MHC was given to the set of genes in mice [75].

MHC was first described as a genetic locus that is related to transplant rejection in mice, yet until 1954, this genetic modulation was not discovered in humans. Jean Dausset and Jan von Rood discovered specific antibodies after analyzing sera from patients with multiple transfusion histories, such as kidney transplant recipients with multiple birth conditions [76–78]. According to their findings, the protein complex was named "human leukocyte antigen", also known as HLA [79].

There are two types of MHC proteins identified in the literature. They diverge according to the protein structure and the different types of cells in which they are expressed. The MHC

protein is named HLA in humans, and the genes encoding this protein family are located on chromosome 6p21 [80]. MHC genes are highly polymorphic due to their nature. Since the MHC protein serves as a plate to present foreign and native antigens to T lymphocytes, the diversity in the protein itself increases the chance of the presentation of a larger number of antigens, which also enhances the survival chance of the organism from an attack of any kind of pathogen; thus, the diversity in the antigen- binding domain of MHC supports this idea [81]. It is shown that the difference between MHC molecules mainly takes place in the antigen- binding domain, specifically where the presenting peptide sequence is bound (Figure 1.3) [82]. The genetic variation in the MHC gene could be observed as evidence of positive selection for the foreign peptide presentation [83]. These unusual point mutations could help maintain dominance [104]. On the other hand, MHC polymorphism could be a result of interallelic recombination and/or gene conversion [85,86]. Exon exchange, along with other genetic changes, could result in an increase in the number of MHC protein variants [84,87].

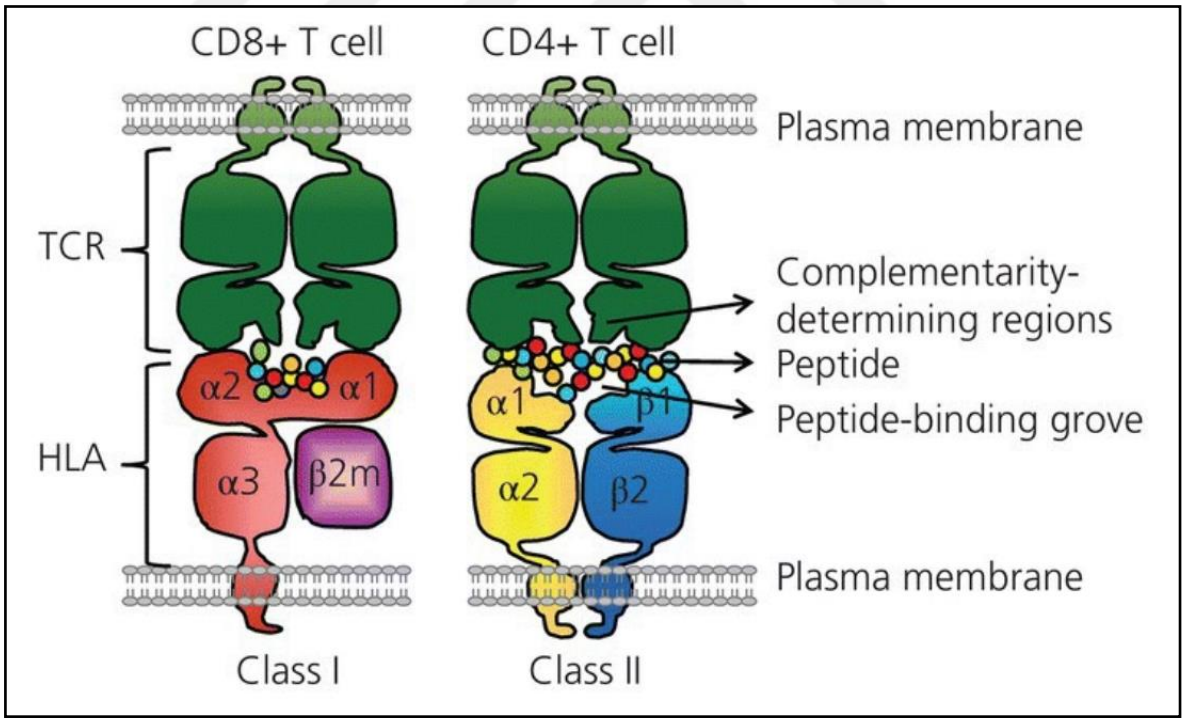

Figure 1. 3. Molecular Structure of MHC I and MHC II [90].

Even though MHC class I and class II molecules have a similar 3D structure, their sequences are less than 20% similar. Both molecules are heterodimers, yet they start to differ with the transmembrane part of the molecule. The MHC class I structure contains the chain, which is

composed of three main fragments: α1, α2, α3, and a soluble β2- microglobulin (β2m) protein. The peptide- binding domain of MHC class I is composed of α1 and α2 fragments and is bound to the membrane through one of α3. The antigen-binding site is very important in MHC molecules since antigen presentation plays a major role in the immune system. β1 and β2 produce a cleft for antigens to click into (Figure 1.3). Two α- helices at the bottom and eight antiparallel β- plated sheets form the cleft. The MHC class II molecule, on the other hand, is made up of two parts and chains that are joined together by their α2 and β2 fragments. The antigen- binding site of MHC class II is composed of α1 and β1 fragments. This antigen- binding site is formed by Ig- like protein folding, which is known to be similar to the MHC class I antigen- binding site [84,91,92].

In the human genome, there are three gene sets for MHC: class I, class II, and class III genes. The MHC class I region contains classical MHC I, nonclassical MHC I, MHC I- like genes, and other immune- related genes. MHC class I genes of the classical class encode proteins such as HLA- A, HLA- B, and HLA- C, which are the primary molecules responsible for presenting antigens to cytotoxic T cells [84]. Their presence also inhibits NK cell activation. Nonclassical HLA genes, on the other hand, are responsible for the expression of HLA- E, HLA- F, HLA- G, and HLA class- I- like proteins such as MHC class I chain- related A (MICA) and MHC class I chain- related B (MICB) [90].

Traditional MHC class I molecules are important for antigen presentation to cytotoxic T cells, but this is not their only function. Classical MHC proteins, MHC class I- related proteins, and non- classical MHC class I proteins could all act as activators or suppressors when interacting with NK cells. NK cells are placed between adaptive and innate immune system cells. They are capable of specifically targeting malignant and infected cell, such as virally infected or oncogenic cells, and initiating the activation of the adaptive immune system through their cytokines and chemokines [91]. NK cells have several different activating and suppressive receptors on their membrane. The regulation of the reactivation also depends on MHC class I molecules as well as other stimulators. One of the NK cell receptors, known as the killer Ig- like receptor (KIR), is the key player in the relationship between MHC class I molecules and NK cell activation. KIR recognizes MHC class I molecules and protects against NK cell attacks. NK cells can kill malignant cells through a

variety of means, including directly killing cells through enzymatic secretions or by inducing apoptosis, similar to cytotoxic T cells [92].

The first HLA- G regulations were identified in cytotrophoblast cells, and they are shown to be pertinent to immune tolerance in the feto- maternal microenvironment [93]. Besides regulation, expression is another important phenomenon that defines the role and importance of HLA- G. Studies showed that HLA- G expressions are observed in tumors [94], allergies [95], virally infected cells, transplanted organs, and autoimmune diseases [96]. Thus, it makes HLA- G a target for immune deficiencies and diseases that need immune regulation either to activate or inactivate the immune system [97]. The HLA- G antigen is important in immune modulation because it inhibits both adaptive and innate immune system cells. The protein's HLA- G1 and HLA- G5 isoforms interact with a variety of inhibitory receptors, including Ig- like transcript- 2 (ILT- 2) and Ig- like transcript- 4 (ILT- 4), as well as the killer cell Ig- like receptor, two Ig domains, and long cytoplasmic tail 4 (KIR2DL4). ILT- 2 has an affinity for classical MHC class I proteins and is expressed in both myeloid and T cells. One of the primary differences between ILT- 2 and ILT- 4 is expression within T lymphocytes, implying that ILT- 2 plays a more complicated role in MHC class I protein regulation than ILT- 4 [98,99]. The KIR2DL4 receptor, on the other hand, is expressed on the surface of NK cells and, more importantly, is an HLA- G ligand [101]. HLA- G complex isoforms, whether soluble or membrane- bound, could inhibit NK cells and induce apoptosis in cytotoxic T lymphocytes [100]. This complex could induce suppressive differentiation in helper T lymphocytes as well as disrupt DC maturation, resulting in T lymphocyte proliferation inhibition [104–107].

The HLA- E molecule is one of the members of the non- classical HLA class I family. They are highly expressed in the immune system, yet they are also known to be expressed to a lesser extent in other types of cells. HLA- E expression was initially explained as being observed in all cell types that express classical HLA class I molecules, despite new research indicating that it is only expressed in lymphoid and endothelial cell types [105,106]. The peptide sequence that is presented on HLA- E differs from classical MHC I molecules. The signal peptide of classical MHC I molecules is cleaved on the endoplasmic reticulum (ER) surface by signal peptide peptidase (SPPase), and part of this cleaved signal peptide is presented on HLA- E to NK cells as a ligand for killer cell lectin- like receptor subfamily C

(CD94/NKG2) [107]. This interaction serves as an inhibitory signal, as it means that the cell could express classical MHC molecules [131–133]. By expressing HLA- E molecules and other self- peptides or pathogenic peptides such as partial viral proteins and structural protein fragments, HLA- E molecules could interact with T cells in general. Last but not least, HLA-F is widely expressed intercellularly in the liver and bladder, and studies show that it helps to maintain classical MHC class I molecule expression [108,109].

HLA class I molecules are known to be heterodimer molecules, which are also integral proteins. However, there are a few cases where HLA class I proteins are observed to be secreted outside of the cell, both in *in vivo* and *in vitro*. These proteins lose their transmembrane fragments due to abnormal splicing in the fifth exon and are secreted outside of the cell [113,114].

Even though it is possible to predict which peptide- MHC complexes will appear following an infection, the mechanism of epitope differentiation from non- epitopes is still unknown [112]. First and foremost, the large number of MHC- peptide complexes could affect the immune response's targeting system [113–115], which is influenced by factors such as MHC- peptide affinity [116], complex stability [117], the efficacy of the MHC antigen process [115,118,119], and the abundance of precursor expressions [114,115,120]. Secondly, the peptide MHC complex needs to be recognized by T lymphocytes because if the MHC- peptide complex could not interact with TCR, the presented peptide could not cause an immune response. Even if all of the conditions are met, the peptide- MHC complex may not be able to elicit an immune response due to the peptide's similarity to a self- peptide [121–123].

MHC class II proteins in humans are called HLA- DR, HLA- DQ, and HLA- DP. These proteins are coded in the same region of the genome (Figure 1.4). The same region also encodes other molecules, such as the antigen processing molecules (HLA- DM and HLA-DO), transporters associated with antigen processing (TAP), and immune proteasome genes (LMP) [124,125]. While they are both antigen- presenting molecules and have similar structures, the MHC class II proteins differ in their function and processing pathways compared to the MHC class I proteins. MHC class II proteins are expressed in very specific

cell types called antigen presenting cells (APCs). There are two types of APCs in the immune system: professional and non- professional APCs. Both groups of cells are known to be immune system cells, such as dendritic cells, B cells, macrophages, mast cells, eosinophils, etc. [126]. These cells phagocytize pathogens and process their proteins to present them over MHC class I proteins for T helper cells to recognize and activate. Endothelial cells, epithelial cells, and lymph node stromal cells (LNSCs), for example, express MHC class II antigen on their surface despite not being derived from hematopoietic progenitors like APCs. Thus, they could support thymocyte development as well as produce an environment for the development of tolerance in the thymus [127].

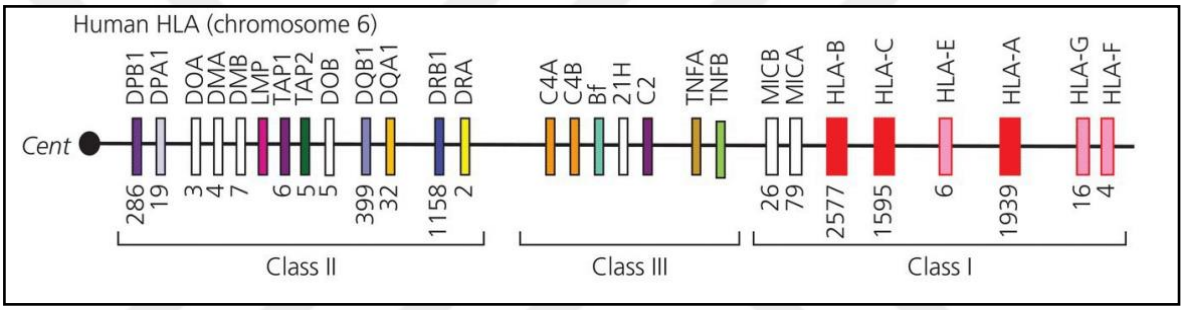

Figure 1. 4. Chromosomal locations of three MHC proteins in humans [80].

Because there are two MHCs, there are two distinct pathways for gene processing across these complexes. For MHC class I molecules, intracellular peptides such as functional cellular proteins and intracellular pathogen proteins, for instance the spike protein of a virus, could be presented to the lymphocytes [128], and MHC class II presents proteins, for instance exergonic antigens derived from bacterial or viral infection or apoptotic bodies [127].

1.2.1.1. Antigen Presentation to CD8⁺ T Lymphocytes through MHC Class I

MHC class I molecules and TCR are the key protein complexes for the immune surveillance of organisms. The presentation of self and non- self- peptides via MHC class I molecules initiates this defense mechanism. Non- self or altered proteins, such as mutagenic proteins, viral proteins, or allogenic proteins, are first degraded into small fragments of peptides by proteosomes [129,130]. These peptide fragments are then digested by cytosolic peptidases, but small sequences survive and bind to TAP, a protein found on the ER membrane [131,132]. With the help of common chaperones such as calreticulin and endoplasmic

reticulum protein 57 (ERp57), small peptide fragments, a special chaperone, TAP, the empty MHC class I molecule forms a loading complex on the ER membrane [133]. TAP assists peptide fragments to attach to empty MHC class I, while tapasin keeps MHC class I in the right conformation for peptide binding. Tapasin also slows down this process, allowing the peptide repertoire to diverge [134]. This process continues until the MHC class I molecule binds to a high- affinity peptide sequence. The length of peptide sequences that could bind to an MHC class I molecule is 6– 8 amino acids. Longer sequenced peptides are cleaved by endoplasmic reticulum aminopeptidase 1 (ERAP1) or, in some organisms, endoplasmic reticulum aminopeptidase 2 (ERAP2) [135–137]. If the peptides that are bound to the MHC class I molecule are longer than 8– 9 amino acids, this triggers ERAP1 to change conformation, which induces trimming of the length of the peptide by hydrolysis. This way, the size of the MHC class I- peptide complex is conserved within optimal conditions [138–140]. Peptides that cannot be presented by the MHC class I molecule are relocated back into the cytoplasm to be recycled [141]. Cytotoxic T cell activation begins with the interaction between the MHC- antigen complex and the TCR. However, the interaction between the MHCI- antigen complex and the TCR is not sufficient for full activation. A co- stimulatory protein called CD8 recognizes the non- antigen- binding side of MHC class I, and this recognition acts as an activator stimulus for the T cell [145]. This activation starts a cascade of processes that result in T cell proliferation. Once the active cytotoxic T cells interact with the specific peptide sequence they are activated against, they use one of two ways to induce cell death. Extrinsic apoptosis is induced by cytotoxic T cells, while enzymes such as perforin and granzyme B actively disrupt cell membrane integrity [53,142,143].

1.2.1.2. Antigen Presentation to $CD4^+$and/or $CD8^+$ T Lymphocytes through MHC Class II

$CD4^+$ and $CD8^+$ T cell activation is mainly induced by TCR and MHC class II interactions between T lymphocytes and APCs. APCs express MHC class II molecules and present either exergonic or endergonic peptides (Figure 1.5) to helper T cells and cytotoxic T cells [144,145]. The peptide fragments that are expressed on MHC class II molecules could be larger than the ones presented on MHC class I molecules, which is one of the differences between these similar complexes [149]. During its assembly in the ER, the MHC class II protein binds to the invariant chain (Ii). This interaction occurs through the part of Ii that is called class Ii- associated invariant chain peptide (CLIP). It resembles a peptide that will be

bound to an MHC class II molecule for the presentation process to T lymphocytes [132,147]. This complex is found in a part of the late endosome called the MHC class II- E- enriched compartment (MIIC) [151,152]. In humans, CLIP is modified with higher- affinity peptide fragments with the help of a chaperone known as DM or HLA- DM [153]. After the alteration of CLIP to a high- affinity peptide, MHC class II molecules loaded with the peptide move to the plasma membrane [151–153].

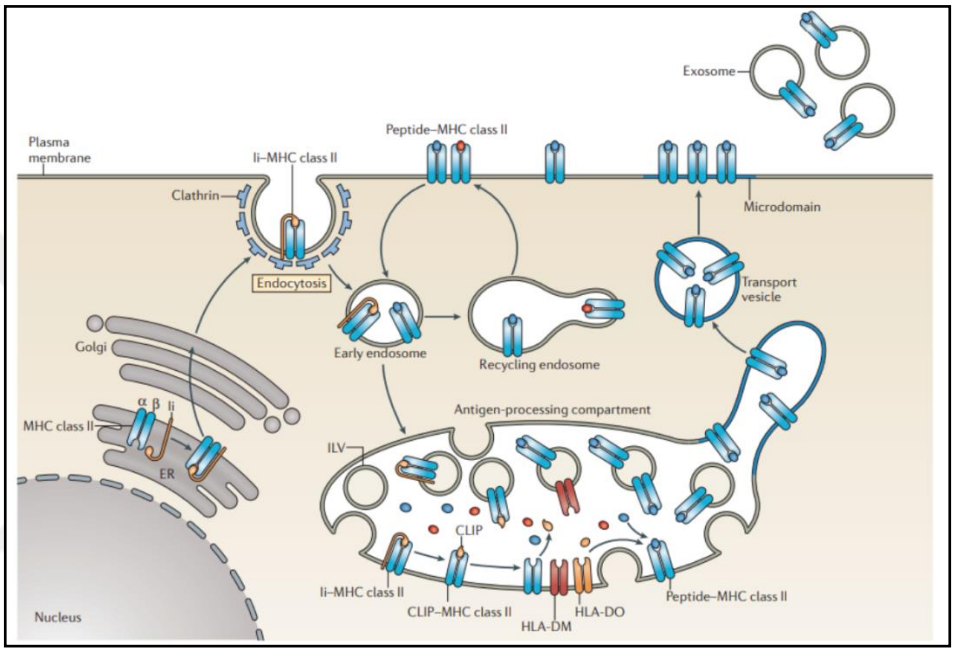

Figure 1. 5. Antigen Processing and Presentation through MHC class II [130].

TCR and MHC II molecules are the main players in T cell activation, but they are not the only protein complexes required for full T lymphocyte activation. There is a diverse set of proteins with different roles, such as co- stimulation, activation, and inhibition. Once a $CD4^+$ or $CD8^+$ T cell recognizes the antigen on the MHC class II molecule, their TCR and a co-stimulatory protein called CD3 interact with MHC II, allowing the first signal for activation to be sent. However, this first signal is inadequate for the full activation of T lymphocytes. In the immune synapse, second signals are required for activator and inhibitor protein interactions. CD80 and CD86 molecules on APCs serve as activators for helper T cells if they interact with CD28 on the T cell surface. On the other hand, the second signal could also cause inactivation through inhibitory proteins such as cytotoxic T lymphocyte-associated protein 4 (CTLA- 4). The interaction between CD80/86 and CTLA- 4 inhibits T cell activation. Full T cell activation necessitates autocrine cytokine stimulation, which is

referred to as the third signal in the T cell activation process. The interaction of CD80/86 and CD28 initiates a series of changes in T cells, resulting in IL- 2 secretion and increased expression of the interleukin- 2 receptor (IL- 2R). IL- 2 induces T cell survival and proliferation [154,155].

1.3. ELECTRIC FIELD

Electric field (EF) applications are often used as an external effect on cells. Effects of EFs on organisms and, on a smaller scale, cells have been observed in different situations (Figure 1.6). Several studies showed that the EF affected many aspects of the cellular system, such as gene expressions and epigenetic modifications [156–158]. Thus, cells that are under a certain amount of EF for a certain period could acquire changes, such as in differentiation capacity [156,159], proliferation [160], viability [161,162], mobility [163,164], and morphology [159,165].

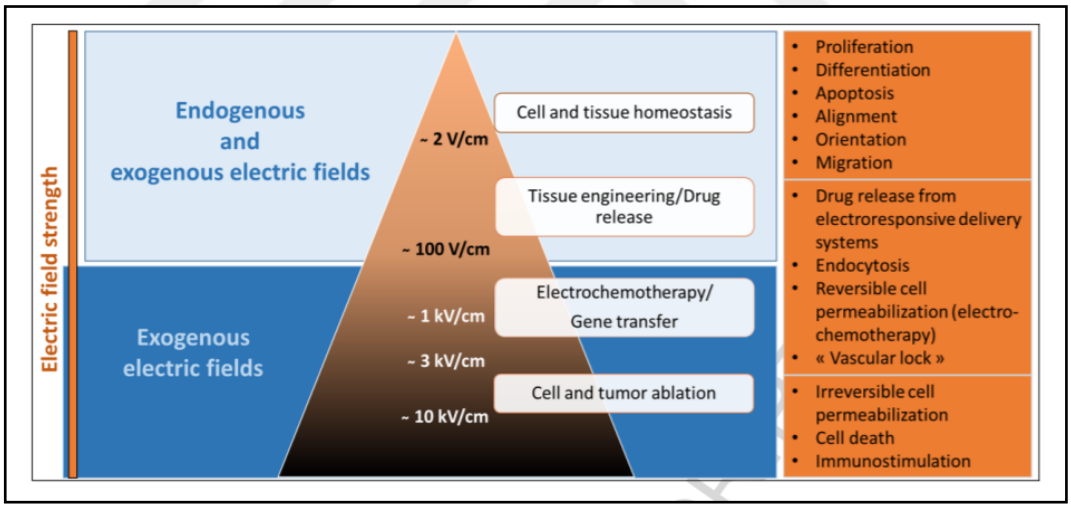

Figure 1. 6. Examples of EF applications and effects [166].

EF applications are generally applied to either polar cells or cells that can differentiate into other cells. Thus, several groups are focusing on the gene expression of differentiation-related transcription factors and migration- related proteins. A study showed that the EF could cause epigenetic alterations due to overexpression of DNA methyltransferase 1 (DNMT1). DNMT1 methylates parts of DNA that encode differentiation- related transcription factors such as OCT4 and NANOG. This is how nanosecond- pulsed EF (nsPEF) enhances the differentiation capacity of mesenchymal stem cells (MSCs) [158].

Cancer cells are also stimulated with an EF to observe if the stimulation has a potential for cancer treatment. In a study concluded in 2007, rats were inoculated intracranially with glioma cells and treated with an EF that has 200 kHz and 2 V/cm magnitude for 6 days. After the treatment, the inoculated tumor was shrunk to half othe size of the control group [168]. Even though EF effects on cancer cells seem to have a future in cancer therapy, the effect they have on normal cells might induce cancerous division, as it could induce cell death in already cancerous cells. According to a 2009 study, the DNA mutation required for tumor growth could not be induced solely by the EF effect on the MRC5 cell line while the cells were also under the effect of 2 gray units of ionizing radiation, which causes severe DNA damage. The outcome showed that DNA damage increased when cells were affected by both ionizing radiation and static electric fields (SEF) [168].

The EF could also affect cell proliferation and viability. In a study focusing on osteoblast cell function under the effects of 0.1 V/cm and 0.5 V/cm expressed EF on MC3T3- T1 cells, proliferation increased with the application of a 0.1 V/cm EF. However, even though proliferation increased by 0.1 V/cm EF, cell- to- cell and cell- to- surface attachment of the mentioned cell type decreased with vinculin and actin stress fiber density [160].

The migration caused by an external EF is called electrotaxis or galvanotaxis [169]. Different cell types were subject to galvanotaxis, such as macrophages, neurons, fibroblasts, epithelial, and endothelial cells. In neurons, EF up to 120 mV/mm migrates towards the cathode, which is close to the physiological EF range [170]. A closer EF magnitude induces elongation in endothelial cells via the vascular endothelial growth factor receptor (VEGFR) pathway [163].

1.3.1. Electric Field and Immune System Cells

The effects of EF on the immune system depend on the nature of the EF in question. In the case of extremely low- frequency electromagnetic fields (ELF- EMF), which have frequencies smaller than 300 Hz, alterations of the blood leukocyte counts [171,172], inflammatory responses [173], modifications to the shape and weight of primary and secondary lymphoid organs, and NK cell activations were observed [174].

Monocytes migrate toward the anode in an EF between 5 mV/mm and 300 mV/mm. Apart from migratory effects, EF induces phagocytic activity in macrophages activating the phosphatidylinositol- 3 kinase (PI3K) and extracellular signal- regulated kinase (ERK) pathways. As a result of the activated pathways, cytokines like tumor necrosis factor- α (TNF- α) are produced and secreted, which improve macrophage function for microbial clearance and healing [175]. NsPEF application to neutrophile cells triggers neutrophil extracellular trap (NET) formation in those cells without an infective element [176]. On the other hand, *in vitro* studies suggest ELF- EMF reduces the secretion of pro- inflammatory cytokines from macrophages due to ELF- EMF's induction of oxidative stress [177]. These two studies show that EF and/or EMF effects can induce two opposite pathways in different immune system cell types.

A study focusing on the effects of nsPEF (0– 60 kV/cm) in Jurkat cells demonstrated that nsPEF could induce apoptosis in Jurkat cells with different cell death pathways. As suggested by Ohtani *et al.* in 2015, exposure to 2.1 GHz radio- frequency (RF) EMF and wideband code division multiple- access signals had an impact on the kinetics, regulation, and helper T cell subtype balance of rat T cells. The thymus and spleen expressed more genes associated with the helper T cell subtype paradigm after exposure to RF EMF, but the protein kinetics and regulation of T cells did not alter [178].

According to Hilpert *et al.*, 500 V/cm of EF is the critical magnitude for the DC population since it reduces the viability and functionality of these cells [180]. Different EF applications demonstrate contrasting results in immune cells; thus, further investigations are required to demonstrate a clear image of the EF effect on the immune system altogether.

1.4. AIM OF THE STUDY

HypoPT is an endocrine system disease that is caused by the Pt tissues' inefficient or lack of secretion of PTH. HypoPT is commonly treated with Pt tissue or cell transplantation. Even though Pt transplantation is the unique permanent treatment method for HypoPT, immune activation- related graft rejection is a common issue in this procedure. Hosts' immune system activation starts with the interaction of HLA surface antigens of transplanted cells to immune cells. In this study, our purpose is to decrease the expression level or stop the expression of HLA class 1 molecules on Pt cells by applying an EF. If we achieve this, the host immune system will be less activated or unactivated. As a result, the success rate of transplantation may increase.

2. MATERIALS AND METHODS

2.1. MATERIALS

2.1.1. Consumables

Table 2. 1. Consumables used in the experiment.

ITEM	BRAND	CATALOG NO
5 mL Serological Pipettes, Polystyrene	Corning Costar	4487
10 mL Serological Pipettes, Polystyrene	Corning Costar	4488
25 mL Serological Pipet, Polystyrene	ISOLAB	I.083.13.025
15 mL Falcon Tubes	Falcon	352096
50 mL Falcon Tubes	Falcon	352070
6 well Plates	Corning Costar	3506
T75 Flask	TPP	90076
T150 Flask	TPP	90151
35 mm x 10 mm Petri Dish	SPL	20035
60 mm x 15 mm Petri Dish	NEST	705001
Double- Sided Tape	Scotch	T1019
Cell Strainer 40 μm	NEST	258369
1050 Alloy Aluminium Plate (99.5% Aluminium, rest another alloying element)	AssanAlüminyum	Free of charge sample from AssanAlüminyum
2.0 mL Cryogenic Vial	NEST	607001
0.2 mL PCR Tubes	Axygen	PCR- 02- C
1.5 mL Eppendorf Tubes	Axygen	MCT- 150- A

2.1.2. Chemicals

Table 2. 2. Chemicals used in the experiment.

ITEM	BRAND	CATALOG NO
10X TBE Buffer	Thermo Scientific	B52
2- Mercaptoethanol	Sigma- Aldrich	M6250- 250ML
2X PCR Master Mix	Thermo Scientific	K0171
6X Loading Dye	Fermentas	R0611
Agarose	Invitrogen	16500- 500
Collagenase Type II	Gibco	17101- 015
DMEM	Gibco	41966- 029
DMEM/F12	Gibco	10565- 018
DMSO	PanReac AppliChem	A3672,0250
DNase I	Roche	101041519001
DPBS 1X	Gibco	14190- 09
FBS	Gibco	10500- 064
GeneRuler DNA Ladder	Thermo Scientific	SM0331
SafeView™	Applied Biological Materials	G108
Trypsin EDTA	Multicell	325- 043- EL
ITS+Premix	Corning	354352
Penicillin Streptomycin (PS)	Gibco	15240- 062
CellROX™ Orange Reagent	Thermo Scientific	C10443
Recombinant Anti- Parathyroid Hormone antibody	Abcam	ab234415
Anti- CaSR antibody	Abcam	ab137408
Goat anti- Mouse IgG (H+L) Cross- Adsorbed Secondary Antibody, Alexa Fluor™ 488	Invitrogen	A- 11001
Goat anti- Rabbit IgG (H+L) Cross- Adsorbed Secondary Antibody, Alexa Fluor™ 488	Invitrogen	A- 11008

2.1.3. Kits

Table 2. 3. Kits used in the experiment.

ITEM	BRAND	CATALOG NO
eBiosceince™ Annexin V-FITC Apoptosis Detection Kit	Invitrogen	BMS500FI- 100
GeneJET RNA Purification Kit	Thermo Scientific	K0732
iScrpit™ cDNA Synthesis Kit	BIO- RAD	1708891
Live/Dead® Viability/Cytotoxicity Kit	Invitrogen	L3224
NucleoSpin® RNA XS	MACHEREY-NAGEL	740902.50
QuantiChrom™ Calcium Assay Kit	BioAssay Systems	DICA- 500

2.1.4. Instruments

Table 2. 4. Instruments used in the experiment.

ITEM	BRAND
Class II Biological Safety Cabinet	Biobase
Cell Culture Incubator	Esco
Centrifuge	Gyrozen
ChemiDOC XRS+Gel Imaging System	BioRad
Flow cytometer B76707 Cytoflex S	Beckman Coulter
Fluorescent Microscope (Axio Vert.A1)	Carl Zeiss
Light Microscope	Carl Zeiss
NanoDrop Spectrophotometer (Nanodrop 200)	ThermoFisher
ProFlex PCR System	Applied Biosystems
Water Bath	N- Biotek
Varioskan LUX Multimode Microplate Reader	ThermoFisher
edge® blu Bluetooth® Smart pH Electrode and Meter	Hanna Instruments

2.2. METHODS

The Pt cells used in this study were provided by Yeditepe University Hospital, Department of Endocrine Surgery. The methodology used in this research was approved by the local human ethics committee, and patients consented to being involved at the beginning of study no: 56733164/203.

Tissue fragments taken from Pt samples were extracted from cases with secondary HyperPT due to chronic renal failure. After the subtotal parathyroidectomy, tissue samples were transferred to Yeditepe University, Thyroid and Parathyroid Research Laboratory in sterile harvest media (serum- free DMEM with 1,000 unit/mL PS).

2.2.4. Pt Cell Isolation

Pt tissue freshly brought from the hospital was separated from connective tissues and adipose tissues, minced into small pieces, and put into a petri dish, which contained 1X DPBS. After mechanical disruption, the tissues were rinsed with 1X DPBS. DPBS was removed before the tissues were placed into an enzyme mix, which contained collagenase type II (1 mg/mL), DNase I (0.05 mg/mL), and bovine serum albumin (BSA) (5 mg/mL) in serum- free RPMI 1640. The falcon tube, which contained the enzyme solution and minced tissue, was placed inside a shaking water bath at 37°C with 80 rpm for 40 min of incubation. Every 10 min, the tissues were harshly agitated via a serological pipette for mechanical disruption of intact parts of the tissue. After incubation, the tissue- enzyme suspension was centrifuged at 500 rpm for 5 min. The supernatant was removed and filtered through a 40 μm pore- size cell strainer, and then centrifuged at 2,000 rpm for 5 min. This process is repeated three times, and each time the pellet was resuspended with DMEM HG (10% FBS, 1% PS). Pt cells were counted and seeded into petri dishes.

2.2.5. Cell Culture

Primary Pt cells were seeded into 35 mm x 10 mm cell culture- treated petri dishes with DMEM HG (10% FBS, 1% PS) (400,000 cells/petri dish). After three days, the media was changed to DMEM/F12 (1% ITS+Premix, 1% PS), and the cells were incubated for 20 h

before being treated with EF. Primary HDF cells were seeded into 60 mm x 15 mm cell culture- treated petri dishes (400,000 cells/petri dish) with DMEM HG (10% FBS, 1% PS). After two days, the cultures were subjected to an EF.

2.2.6. Electric Field Application and Sample Collection

The media of Pt cells were changed 20 h before the experiment and collected for PTH measurement right before the EF application. The collected media was centrifuged at 4,000 rpm for 15 min, and samples were collected for PTH measurement from the supernatant.

Petri dishes, where Pt and HDF cells were seeded separately, were placed on an aluminium plate with the help of double- sided tape, and another aluminium plate was placed on top of the petri dishes as shown in Figure 2.1. The positive voltage source was attached to the bottom plate, and the negative voltage source was bound to the top plate. The space between two plates was 2 cm. An EF with 600 V and 1200 V electric sources was applied individually to Pt and HDF cells for 1 h.

Pt cell media was collected 20 h after EF application, and the collected samples were prepared as previously described. PTH samples collected 20 h before and after the EF application were sent to the biochemistry laboratory for ELISA testing.

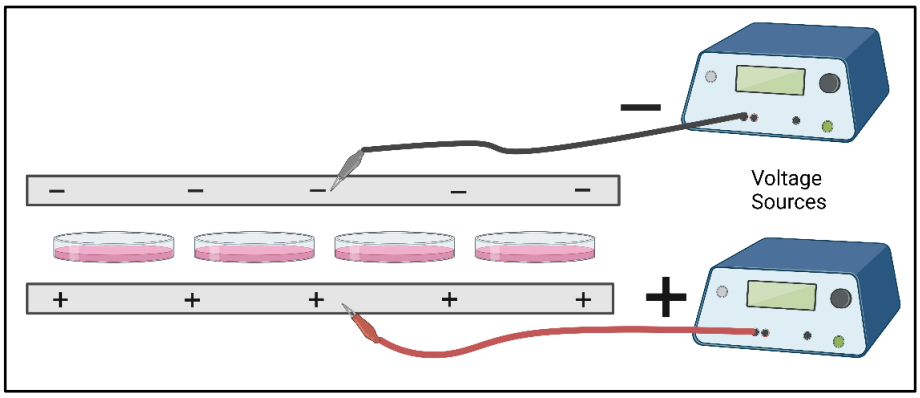

Figure 2. 1. Schematic Design of EF Application.

2.2.7. Annexin- V and Propidium Iodide (PI) Assay

The effect of the EF on the viability of HDF and Pt cells was determined using the eBiosceince™ Annexin V- FITC Apoptosis Detection kit, and the manufacturer's protocol was followed. After EF application, cells were cultured for 24 h prior to collection and rinsed with ice- cold 1X DPBS before being resuspended in 195 µL of 1X Annexin- V Binding Buffer and 5 µL of Annexin- V FITC. Samples were incubated for 10 min at room temperature (RT). Following incubation, the samples were centrifuged at 2,000 rpm for 5 min, washed once with 200 µL 1X Annexin- V Binding Buffer, and finally resuspended again in 190 µL 1X Annexin- V Binding Buffer. PI (10 µL) were briefly added to the samples before flow cytometry analysis. The CytExpert analysis program was used to analyse the flow cytometer B76707 Cytoflex S data.

2.2.8. Live/Dead Assay

Live/Dead® Viability/Cytotoxicity Kit (Invitrogen, USA) protocol was applied to the cells after 48 h and 72 h of EF application. The media of Pt and HDF samples that were in 30 mm x 10 mm petri dishes were removed, and cells were rinsed with 1X DPBS solution. The working solution was prepared with 2 µM Calcein- AM and 4 µM Ethidium Homodimer- 1 containing 1X DPBS, and samples were incubated in this working solution for 30– 45 min. After the incubation, the working solution was removed, and petri dishes were rinsed with 1X DPBS. The samples were visualized using a fluorescent microscope (Axio Vert.A1).

2.2.9. RNA Isolation

The effects of EF on gene expression in HDF and Pt cells were determined by polymerase chain reaction. Thus, the total RNA of both HDF and Pt cell groups was isolated with two different protocols.

The total RNA of Pt cell samples was isolated with NucleoSpin® RNA XS according to the protocol suggested by the manufacturer. Cells were removed from petri dishes using trypsin/EDTA. A working solution containing 100 µL of RA1 solution and 2 µL of TCEP was added to the samples, which were centrifuged and vortexed. Afterwards, a 5 µL carrier

RNA- containing working solution was prepared, which contained 20 ng carrier RNA, and vortexed again. Samples were mixed with 100 µL of 70% (v/v) ethanol, and samples were transferred to NucleoSpin® RNA XS columns. After the transfer, the samples were centrifuged at 11,000 rpm for 30 sec. The supernatant was removed, and 100 µL of MDB was added to the samples before another centrifugation at 11,000 rpm for 30 sec. The supernatant was discarded again, and the samples were incubated with 25 µL of DNase reaction mix for 15 min. After 2 min of incubation, washing steps began with 100 µL of RA2 buffer and continued with 400 µL of RA3 buffer. Samples were centrifuged at 11,000 rpm for 30 sec, and the supernatants were discarded. At the last washing step, 200 µL of RA3 buffer was added to the samples and centrifuged at 11,000 rpm for 2 min. The columns were placed in a collection tube, and 10 µL of RNase- free H_2O was added to the columns. Samples were centrifuged for 30 sec at 11,000 rpm. Concentrations and purity of total RNA were measured with NanoDrop spectrophotometry.

Total RNA from HDF cells was isolated using the GeneJET RNA Purification Kit according to the manufacturer's protocol. HDF cell samples were removed from petri dishes and rinsed with trypsin/EDTA to remove any remaining media. Samples were vortexed for 10 sec in 600 µL Lysis buffer, which contained 2.86 M 2- Mercaptaethanol. Then 360 µL of 96% (v/v) ethanol was added, and 700 µL of the samples were transferred to a GeneJET RNA Purification Column. The columns were centrifuged for 1 min at 12,000 rpm, and the supernatant was discarded. The same step was applied to the rest of the samples. After the centrifugation, 700 µL of Wash Buffer 1 was added into the columns and centrifuged at 12,000 rpm for 1 min. The washing step continued with 600 µL Wash Buffer 2 and centrifugation at 12,000 rpm for 1 min and 200 µL Wash Buffer 2 and centrifugation at 12,000 rpm for 2 min. Lastly, the columns were placed into a collection tube, and 40 µL of nuclease- free water was added to the samples. The columns were centrifuged at 12,000 rpm for 1 min. After the collection of total RNA, concentration and purity measurements were performed with NanoDrop spectrophotometry.

2.2.10. Polymerase Chain Reaction and Gel Electrophoresis

Isolated total RNA samples from Pt and HDF cells were used individually to produce template DNA for Polymerase Chain Reaction. Samples were prepared according to Table

2.5. Instructions from the manufacturer were followed along with the procedure. Samples were incubated at 25°C for 5 min, 46°C for 20 min, and 95°C for 1 min, respectively in the thermocycler.

Table 2. 5. Reverse Transcription (RT)- PCR protocol components.

Component	**Volume**
5X iScript Reaction Mix	5 µL
iScript Reverese Transcriptase	1.25 µL
Nuclease- free Water	Variable
RNA (100 ng)	Variable
Total Volume	25 µL

Following the synthesis of DNA templates with the iScrpit^{TM} cDNA Synthesis Kit, polymerase chain reaction (PCR) was performed with protocols suggested by the manufacturer, using the components and reagents that are shown in Table 2.6, to determine the gene expression profile of HLA class I molecules, PTH, and GCM2 before and after EF application with different voltage sources. Glyceraldehyde- 3- Phosphate Dehydrogenase (GAPDH) was chosen as the reference gene for the normalization of the specific gene expressions. The polymerase chain reaction was carried out in the thermocycler according to the protocol shown in Table 2.7, and Table 2.8 shows the forward and reverse primer sequences, as well as the expected lengths of the gene outcomes and the optimized reaction temperature.

Table 2. 6. PCR protocol components.

Components	Volume
DNA Template	3 µL
PCR Mix (2X)	6.3 µL
Nuclease- free Water	2.5 µL
Primer (Forward and Reverse)	0.7 µL (0.35 µL Forward, 0.35 µL Reverse)
Total Volume	12.5 µL

Table 2. 7. PCR protocol.

Step	Temperature (°C)	Time	Cycle
DNA Denaturation and Polymerase Activation	95	1 min	1
Denaturation	95	30 sec	35
Annealing	52 and/or 56	30 sec	
Extension	72	1 min	

Table 2. 8. Forward (F) and Reverse (R) primer sequences with the expected length of the outcome and optimized temperature.

Primers	Sequences (5'→3')		Product Length (bp)	Optimized Temperature (°C)
GAPDH	F	AACGTGTCAGTGGTGGACCTG	160	56
	R	AGTGGGTGTCGCTGTTGAAGT		
HLA- A	F	TCTTTGGAGCTGTGATCACT	197	51
	R	AAGGGCAGGAACAACTCTTG		
HLA- B	F	ATTACATCGCCCTGAACGAG	274	51
	R	ATCTCCCGCAGGGTAGAAACC		
HLA- C	F	TCCTGGTTGTCCTAGCTGTC	151	51
	R	CAGGCTTTACAAGTGATGAG		
PTH	F	GACATTGTATGTGAAGATGATACC	191	56
	R	GCTTCTTACGCAGCCATTCTA		
GCM2	F	CACCTGGCACCTGTCCTTTTTTC	295	56
	R	GGCCATTGTGGTTGTTGGTGTTGCG		

For the visualization of PCR products, a 250 mL 2% (w/v) agarose gel was prepared with 1X TBE buffer using 12 µL SafeView™. PCR products of 10 µL were mixed with 2 µL of

6X loading dye and loaded into a 2% (w/v) agarose gel. The gel was run for 1 h under 110 V. The gel image was taken with the ChemiDOS XRS+Gel Imaging System.

2.2.11. Oxidative Stress Detection

Control (0 V), 600 V, and 1200 V samples were rinsed with 1X PBS before the protocol. Pt cells were stained with 5 μM CellROX™ Orange Reagent in 1X PBS for 30 min in the dark. After the incubation, the cells were rinsed with 1X PBS three times. Then they were analysed by the flow cytometer B76707 Cytoflex S.

2.2.12. Immunofluorescent Staining

Pt cells were seeded 2 days before the staining protocol at a density of 10,000 cells per petri dish. These cells were rinsed with 1X PBS before starting immunofluorescence staining. Table 2.9 demonstrates the steps of the protocol. Samples were drained from the media and rinsed with 1X PBS before fixation with 3.7% (v/v) formaldehyde for at least 1 h. After fixation incubation, samples were rinsed with 1X PBS, and for PTH, samples were permeabilized with 0.1% Triton- X 100 for 5 min. PTH samples were rinsed with 1X PBS, and then both PTH and CaSR samples were incubated with a blocking solution (3% (v/v) FBS in PBS) for 10 min. Samples were stained separately with PTH and CaSR primary antibodies for 1 h. Samples were rinsed with 1X PBS and then stained with secondary antibodies. The protocol was followed in the dark from this point on. Samples were rinsed with 1X PBS, and then they were stained with DAPI for 15 min. The samples were visualized with the assistance of a fluorescent microscope (Axio Vert.A1) using DAPI (blue) and FITC (green) filters.

Table 2. 9. Immunofluorescent Staining Protocol.

Step	Time
Fixation (3.7 % (v/v) Paraformaldehyde in 1X PBS)	At least 1 h
Permeabilization (0.1 % Triton- X 100 (v/v) in 1X PBS)	5 min
Blocking (3 % (v/v) FBS in 1X PBS)	10 min
Primary Antibody Staining (1:200 for PTH, 1:1000 for CaSR prepared in antibody preparation solution- 1.5 % (v/v) FBS in 1X PBS)	1 h
Secondary Antibody Staining (1:2000 (v/v) for PTH Goat anti-Mouse IgG (H+L) Cross- Adsorbed Secondary Antibody, Alexa Fluor™ 488 , 1:1000 (v/v) for CaSR Goat anti- Rabbit IgG (H+L) Cross-Adsorbed Secondary Antibody, Alexa Fluor™ 488 in antibody preparing solution)	45 min
DAPI Staining (1:1000 (v/v) in antibody preparing solution)	15 min

Seeded cells were rinsed with PBS before starting PTH and CaSR. The permeabilization step was skipped for CaSR staining. The samples were visualized with the assistance of a fluorescent microscope (Axio Vert.A1).

2.2.13. Ca^{2+} Ion Detection

For the possible effect of EF on the calcium influx of Pt cells, a calcium detection assay was applied. For this experiment, QuantiChrom™ Calcium Assay Kit was used, and the manufacturer's suggested protocol was followed. Control (0 V), 600 V, and 1200 V samples' media were collected after 1 and 20 h of incubation. Media samples were added to a 96–well plate in a volume of 5 µL, and a working reagent was prepared by combining equal amounts of reagents A and B. After mixing, 200 µL working reagent was added directly to the samples. After 3 min of incubation in the dark, the absorbance of the samples and standard was measured at 612 nm with a Varioskan LUX Multimode Microplate Reader. A standard curve was drawn, and according to this curve, the concentration of the samples' calcium (mg/dL) was calculated.

2.2.14. pH Detection

A pH detection method was utilized to assess the possible effect of EF on the pH of the media. For this experiment, a pH meter (Hanna Instruments) was used. Before measuring the pH of the samples, the pH meter was calibrated with standard solutions (pH:4, 7, and 10).

2. RESULTS

3.1. PT CHARACTERISATION

Pt cells were isolated from fresh Pt tissues, and the characterization of these cells was determined by Pt specific features using three different techniques: PTH secretion using PTH ELISA kit, CaSR and PTH protein detection using immunofluorescent staining, and PTH and GCM2 gene expressions using PCR.

The ELISA assay was applied to the media collected from Pt cells after isolation to determine the PTH secretion function of isolated cells. As shown in Figure 3.1, isolated Pt cells demonstrated 711.1 ± 20.92 pg/mL of PTH in their media.

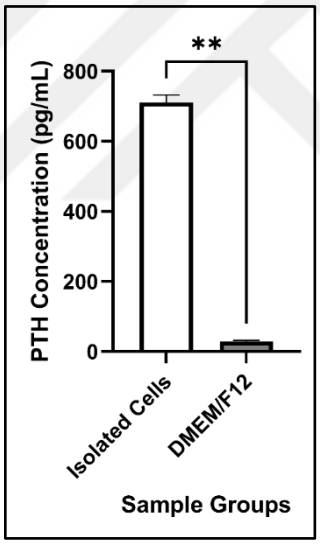

Figure 3. 1. PTH secretion from isolated Pt cells 3 days after isolation. Media from isolated cells from parathyroid tissue and cell- free media were used to compare PTH concentrations. A two- tailed student t- test was performed for statistical analysis. *p<0.05, **p<0.01, ***p<0.001, and ****p<0.0001 (n=9 for each group).

An immunofluorescent staining was applied to Pt cells after isolation to determine the characteristic properties of isolated cells. CaSR and PTH proteins were selected for the conformation of the Pt characteristic of these cells. Figures 3.2 and 3.3 demonstrate that isolated Pt cells express both CaSR and PTH.

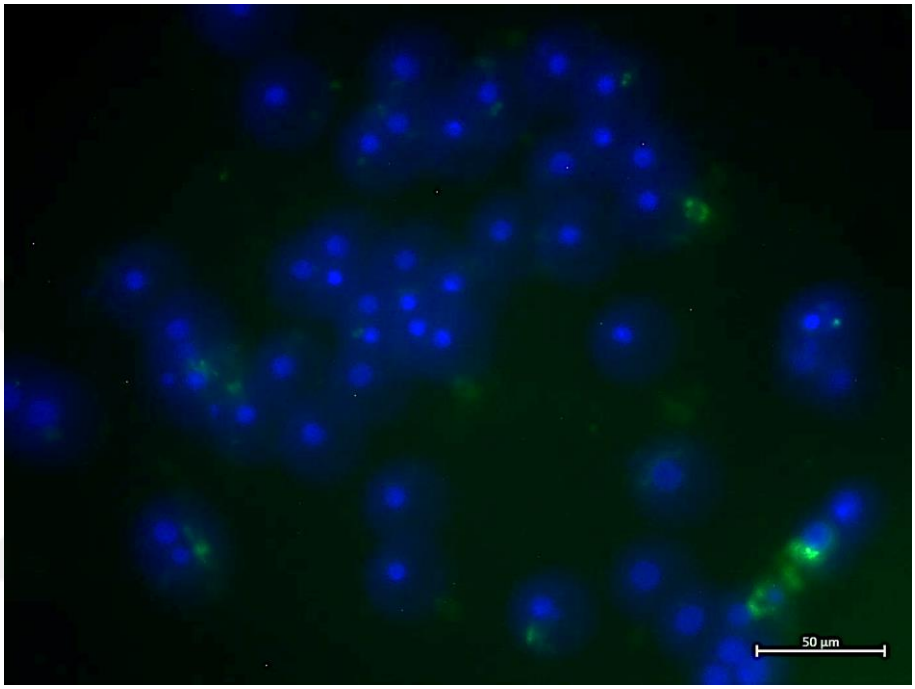

Figure 3. 2. Immunofluorescent staining of isolated PTH applied to Pt cells. The blue colour demonstrates the nucleus of the cells using DAPI, and the green colour demonstrates PTH as an internal protein (Scale bar demonstrated in the figure is 50 µm).

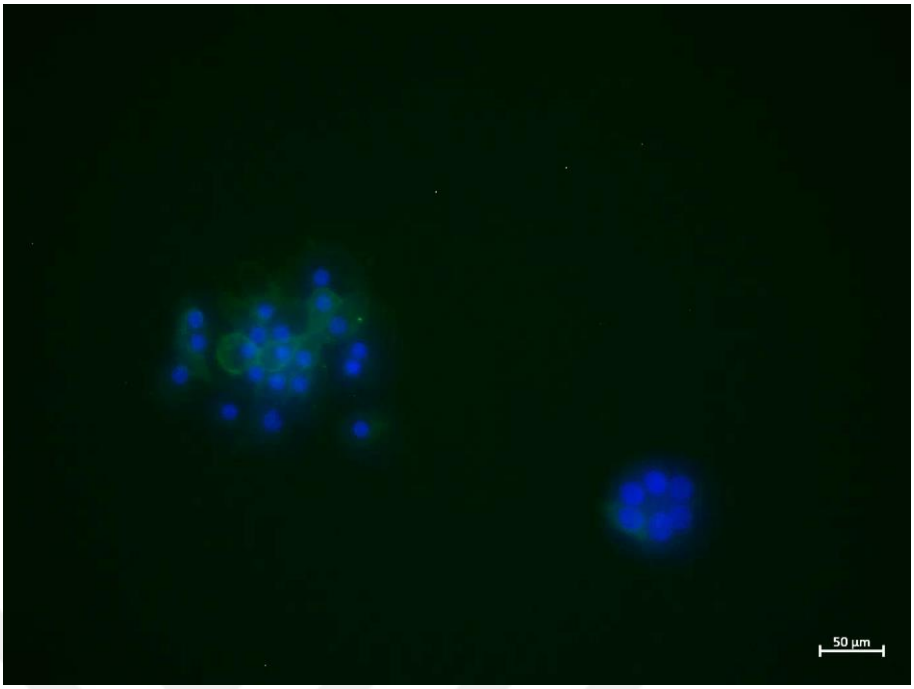

Figure 3. 3. Immunofluorescent staining of CaSR applied to isolated Pt cells. The blue colour demonstrates the nucleus of the cells using DAPI, and the green colour demonstrates the CaSR surface protein (Scale bar demonstrated in the figure is 50 µm).

For gene expression, Figure 3.4 demonstrates that isolated cells express both GCM2 and PTH. GCM2, which is a transcription factor essential for Pt gland development and PTH expression in isolated cells, expressed that these cells are Pt cells. GAPDH was used as a housekeeping gene.

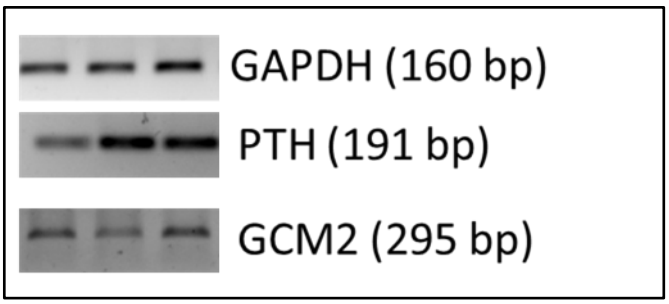

Figure 3. 4. Gel image of GAPDH, PTH, and GCM2 gene expressions in isolated Pt cells.

3.2. FLOW CYTOMETRY ANALYSIS OF ANNEXIN- V AND PROPIDIUM IODIDE (PI) ASSAY

The viability of the HDF and Pt cells 24 h after EF application was estimated with the assistance of Annexin- V and PI in flow cytometry. Annexin- V- stained cells demonstrated early apoptotic cells, and PI- stained cells demonstrated necrotic cells. In Figures 3.5 and 3.7, double- positive (upper right) cells indicated late apoptotic cells. In the same figures, viable cells were shown in the double- negative part (lower left) of this assay. For the analysis of this assay, the CytExpert program was used.

The viability of HDF and Pt cells after EF application was determined with Annexin- V and PI assay. EF was not used in the cells of the Control (0 V) group. The cell population was determined by the granularity and cell size of the sample. The results obtained from Figures 3.5 and 3.6 are shown in Tables 3.1 and 3.2. After the applications, the approximate viability of HDF cell groups was detected as being 85.59% ± 0.029 for the Control (0 V) group, 86.13% ± 0.009 for the 600 V, EF, and 87.67% ± 0.006 for the 1200 V, EF. The groups' viability was expected to be close to one another. The control group's early apoptotic cell population was 12.71% ± 0.028 in the Control (0 V) group, 12.14% ± 0.004 in the 600 V group, and 10.96% ± 0.006 in the 1200 V group. For the late apoptotic cell population, groups demonstrated the results as follows: 1.30% ± 0.004 for the Control (0 V) groups, 1.18% ± 0.004 for the 600 V groups, and 0.89% ± 0.004 for the 1200 V groups.

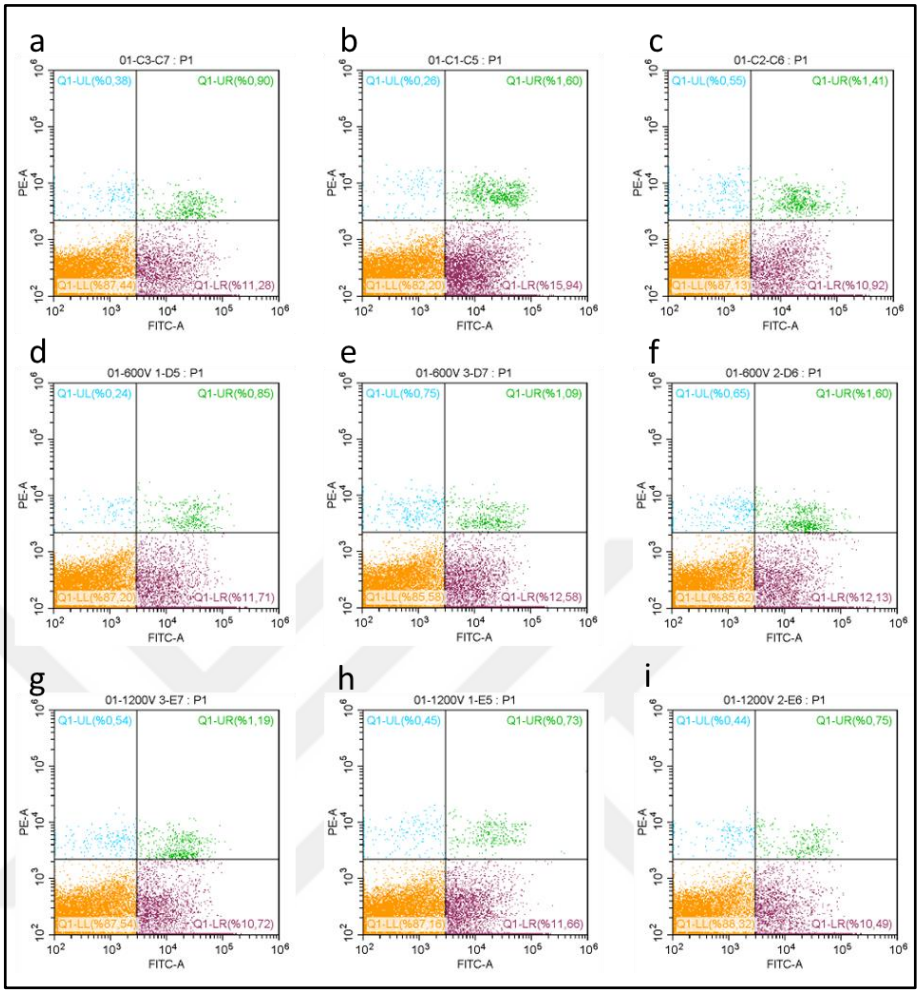

Figure 3. 5. Flow cytometry- assisted Annexin- V and PI assay of HDF cells 24 h after application: Control (0 V) (a, b, and c), 600 V (d, e, and f), and 1200 V (g, h, and i). The quadrate dot plot was used to illustrate only the double- negative, Annexin- V positive, PI positive, and double- positive cell populations. The lower left (orange dots) represents the double- negative cells, which are also indicated as living cells. The green dots on the upper right represent double- positive cells, which are a population of late apoptotic cells. The upper left (blue dots) and lower right (purple dots) populations show which cells are necrotic and early apoptotic, respectively.

Table 3. 1. Annexin- V and PI evaluations after 24 h of incubation: Control (0 V), 600 V, and 1200 V EF to HDF cells for 1 h application (n=3 for each group).

Samples	Alive	Early Apoptosis	Late Apoptosis	Necrosis
Control (0 V)	85.59% ± 0.03	12.71% ± 0.03	1.30% ± 0.01	0.40% ± 0.01
600 V	86.13% ± 0.01	12.14% ± 0.01	1.18% ± 0.01	0.55% ± 0.01
1200 V	87.67% ± 0.01	10.96% ± 0.01	0.89% ± 0.01	0.48% ± 0.01

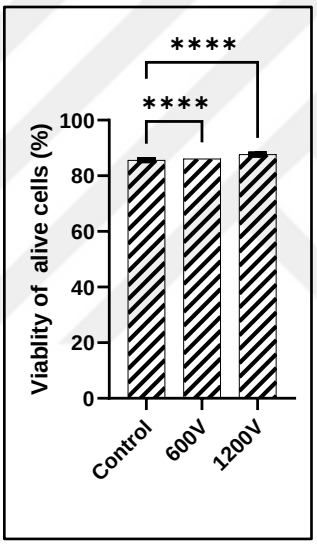

Figure 3. 6. Graphic of Annexin- V and PI evaluations after 24 h of incubation: Control (0 V), 600 V, and 1200 V EF to HDF cells for 1 h application. To determine the significant difference in sample viability, a one- way ANOVA (Dunnett's multiple comparison test) was used: *p<0.05, **p<0.01, ***p<0.001, and ****p<0.0001 (n = 3 for each group).

To determine the potential lethal effect of EF application, the highest voltage was increased up to 5000 V, and EF was applied first to HDF cells as a model cell population for 1 h. The annexin V/PI assay was used for the demonstration of the apoptotic and necrotic effects of EF 24 h after application. In Figure 3.7, the dot plots illustrate the results of the analysis. Since this was a preliminary experiment, the sample size was n=2 for each group. The alive cell population in Control (0 V) groups was 91.93% ± 1.51, and in the 5000 V EF applied groups, 92.52 ± 0.20 of the cells were alive. EF application with 5000 V did not promote

apoptotic and/or necrotic activity in HDF cells. Since higher voltages than 5000 V would be dangerous for the experiment, a lethal voltage dosage could not be detected. The EF application protocol was followed with 600 V and 1200 V sources due to their promising preliminary data.

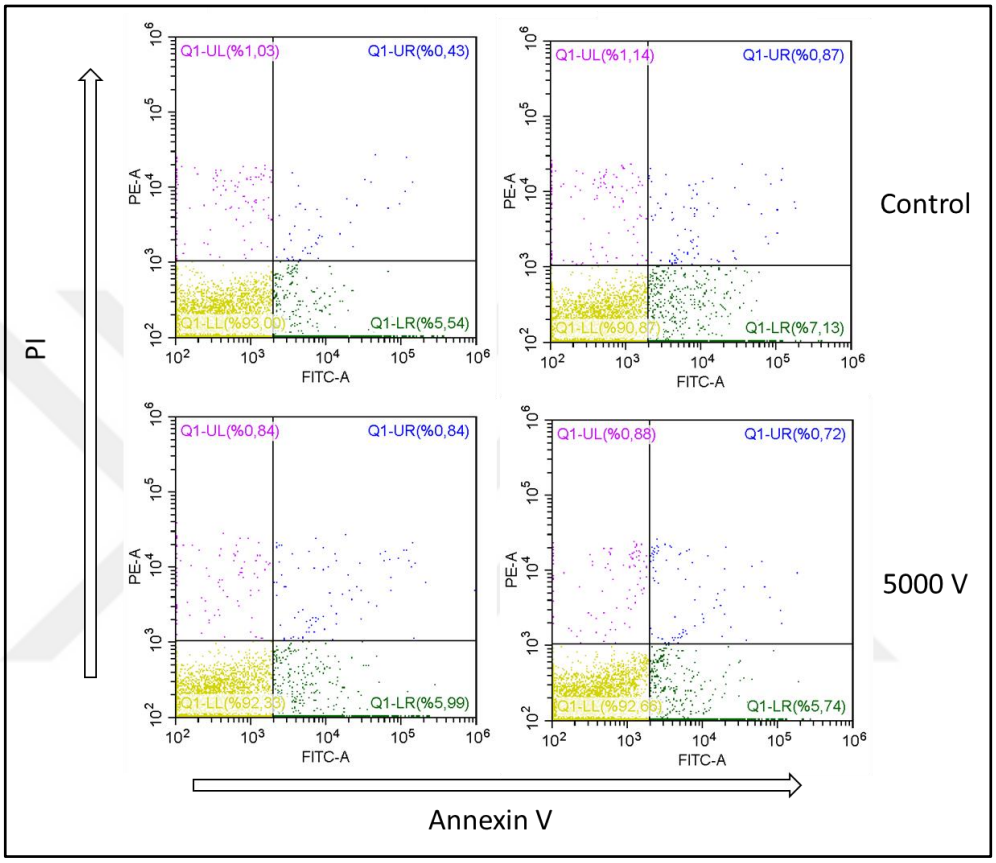

Figure 3. 7. Flow cytometry- assisted Annexin- V/PI assay of HDF cells 24 h after EF application: Control (0 V) and 5000 V. The quadrate dot plot was used to illustrate the double- negative, Annexin- V- positive, PI- positive, and double- positive cell populations. The lower left (yellow) represents the double- negative cells, which are also indicated as living cells. The blue dots on the upper right represent double- positive cells, which are a population of late apoptotic cells. The upper left (pink dots) and lower right (green dots) populations show which cells are necrotic and early apoptotic, respectively.

The results obtained from Figures 3.8 and 3.9 are shown in Table 3.2. After the applications, the approximate viability of Pt cell groups was detected as being 52.84% ± 0.09 for the Control (0 V) group, 49.44% ± 0.03 for the 600 V EF, and 40.50% ± 0.05 for the 1200 V EF. The early apoptotic cell population in the Control (0 V) group was 4.21% ± 0.01; in the

600 V group, 3.71% ± 0.01; and in the 1200 V group, 4.19% ± 0.01. For the late apoptotic cell population, groups demonstrated the results as follows: Control (0 V) group: 24.28% ± 0.06, 600 V groups: 25.63% ± 0.02, 1200 V groups: 31.15% ± 0.04.

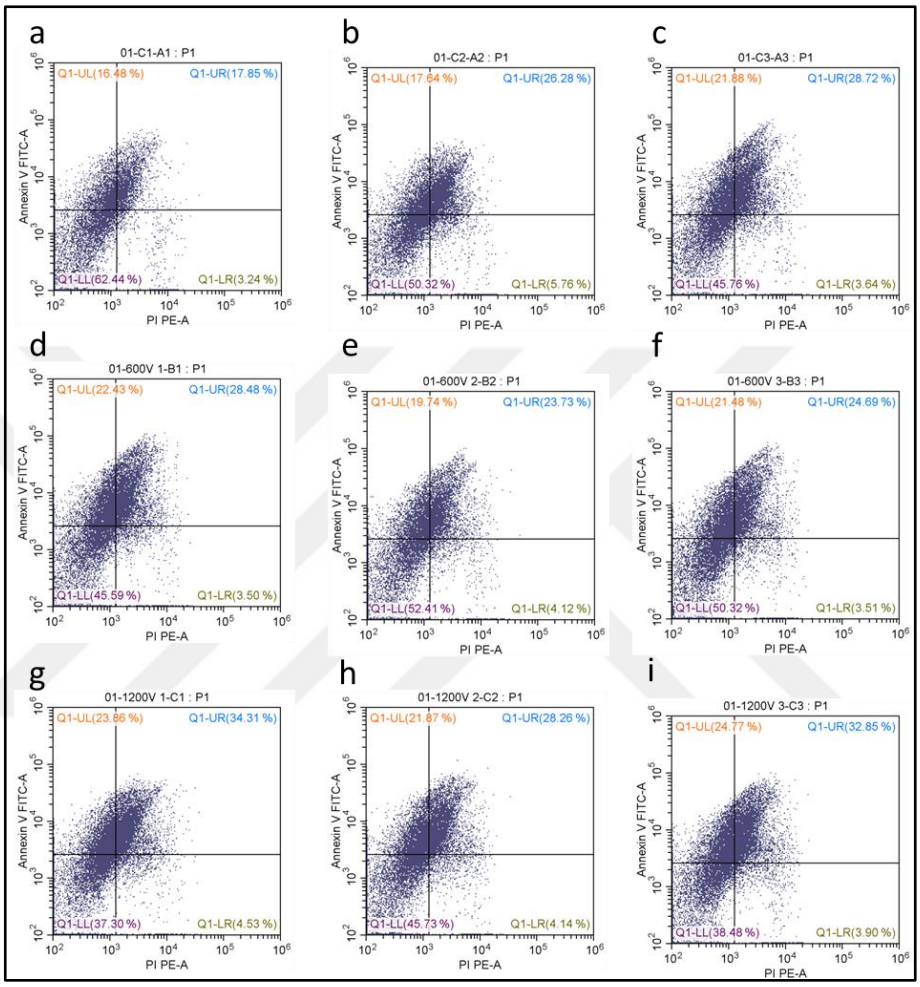

Figure 3. 8. Flow cytometry- assisted Annexin- V and PI assay of Pt cells 24 h after application: Control (0 V) (Figures 3.1.a, b, and c), 600 V (Figures 3.1.d, e, and f), and 1200 V (Figures 3.1.g, h, and i). The quadrate dot plot was used to illustrate the double-negative, only- Annexin- V positive, only- PI- positive, and double- positive populations. The lower left shows the double- negative, which is also indicated as alive cells. The upper right shows the double- positive cell population that shows the late apoptotic cells. The lower right and upper right populations determine the necrotic and early apoptotic cell populations, respectively.

Table 3. 2. Annexin- V and PI assay evaluations of Control (0 V), 600 V, and 1200 V Pt cells after 1 h application (n=3 for each group).

Samples	Viability	Early Apoptosis	Late Apoptosis	Necrosis
Control (0 V)	52.84% ± 0.09	4.21% ± 0.01	24.28% ± 0.06	18.67% ± 0.03
600 V	49.44% ± 0.03	3.71% ± 0.01	25.63% ± 0.02	21.22% ± 0.01
1200 V	40.50% ± 0.05	4.19% ± 0.01	31.15% ± 0.04	23.50% ± 0.01

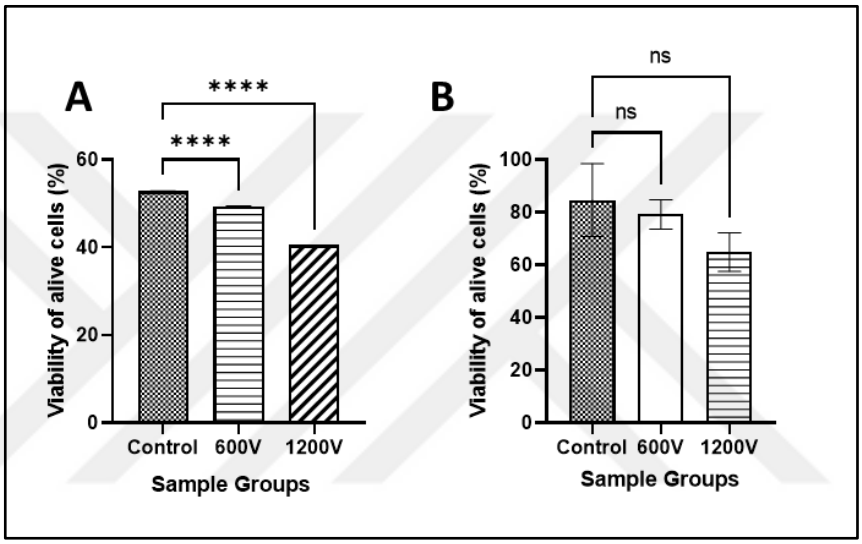

Figure 3. 9. (A) Graphic of Annexin- V and PI evaluations after 24 h of incubation: Control (0 V), 600 V, and 1200 V EF to Pt cells for 1 h application (B) Relative viability graphic of Pt after 24 h of incubation: Control (0 V), 600 V, and 1200 V EF to Pt cells for 1 h application. To determine the significant difference in sample viability, a one- way ANOVA (Dunnett's multiple comparison test) was used: *p<0.05, **p<0.01, ***p<0.001, and ****p<0.0001 (n = 3 for each group).

3.3. LIVE/DEAD ASSAY

The Live/Dead assay was applied to HDF cells and Pt cells at 48 h and 72 h after 1 h of EF application with Control (0 V), 600 V, and 1200 V electric sources. The green fluorescence indicates that the cells are alive, whereas the red fluorescence indicates that the cells are dead. The images shown in Figures 3.10 and 3.11 were taken by fluorescent microscopy.

The viability of HDF and Pt cells was Controlled after 48 and 72 h incubation, respectively. The viability of the cells after 1 h of EF application at 600 V, and 1200 V did not change when compared with the Control (0 V) group. Green- labelled cell populations shown in Figures 3.10 and 3.11 indicate alive cells.

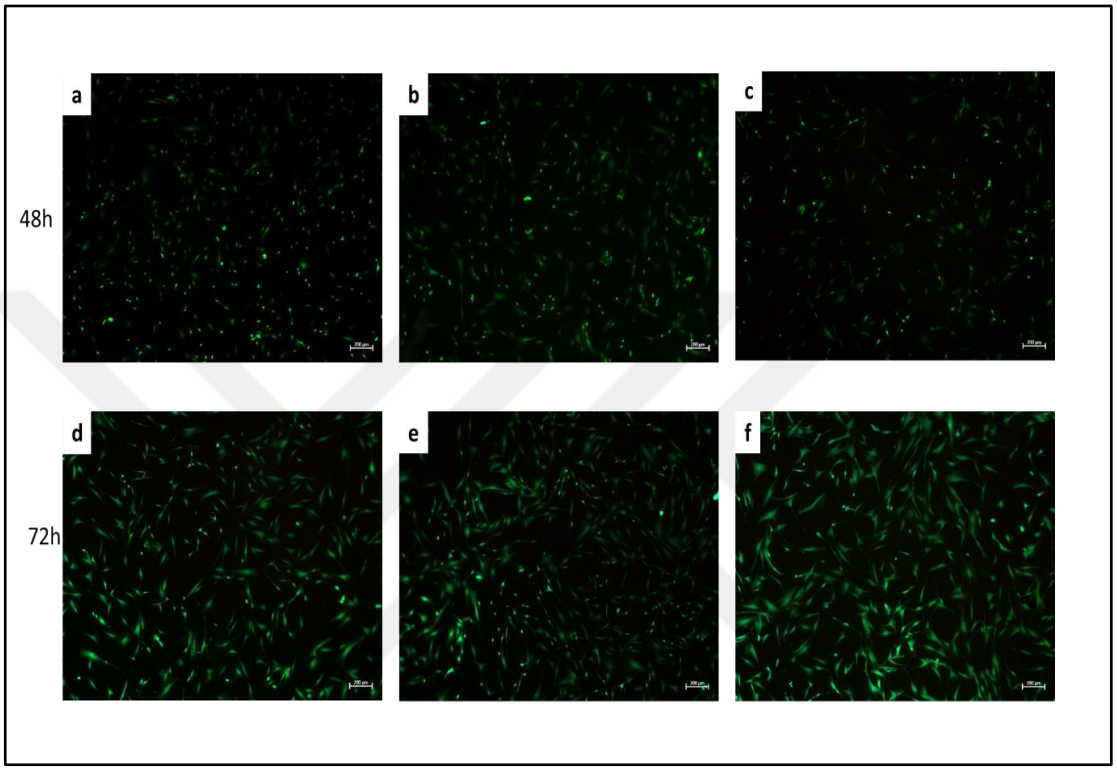

Figure 3. 10. Live/Dead Viability assay applied to HDF cells after 48 h of incubation: Control (0 V) group (a), 600 V group (b), 1200 V group (c), and 72 h of incubation: Control (0 V) (d), 600 V group (e), and 1200 V group (f).Green colour demonstrates alive cells, and red colour demonstrates dead cells (Scale bar demonstrated in the figure is 200 μm).

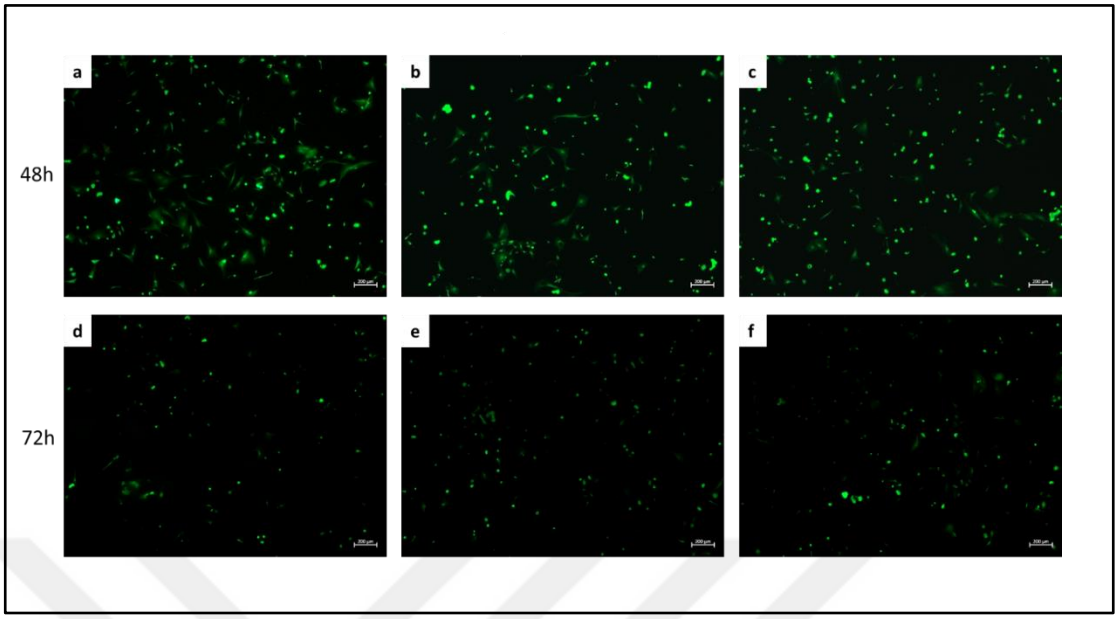

Figure 3. 11. Live/Dead Viability assay applied to Pt cells after 48 h of incubation: Control (0 V) group (a), 600 V group (b), 1200 V group (c), and 72 h of incubation: Control (0 V) (d), 600 V group (e), and 1200 V group (f). Green colour demonstrates alive cells, and red colour demonstrates dead cells (Scale bar demonstrated in the figure is 200 μm).

3.4. POLYMERASE CHAIN REACTION

After EF application, samples were incubated for 10 days, and then RNA was isolated from the respective samples. Gene expression in HDF and Pt cells was determined by PCR and gel electrophoresis. The analysis of gel electrophoresis images was visualized with the assistance of the ChemiDOC XRS+Gel Imaging System shown in Figures 3.12 and 3.14, and the normalization and fold change analysis were applied by the ImageJ system. The GAPDH gene was selected as the reference gene for the normalization of gene expressions. Fold- change graphics were demonstrated in Figures 3.13 and 3.15.

Classical HLA class I complex isoform expression after 1 h of EF application with 600 V and 1200 V electric sources to HDF cells was determined regarding GAPDH normalization. The same normalization housekeeping genes were used for the PTH, GCM2, and classical HLA class I isoform expressions after 1 h of EF application with 600 V, and 1200 V electric sources to Pt cells. Following 600 V and 1200 V EF applications, HLA- A expression decreased by 0.63 ± 0.038 and 0.35 ± 0.145; HLA- B expression decreased by 0.99 ± 0.087

and 0.84 ± 0108; and HLA- C expression decreased by 0.60 ± 0.039 and 0.26 ± 0.068 folds, respectively, when compared to the Control group (0 V). The decrease could be observed visually from the gel electrophoresis, as shown in Figure 3.12, and after normalization, as calculated fold- change data in Figure 3.13 graphics. The statistical data was obtained from the gel images with the assistance of the ImageJ program.

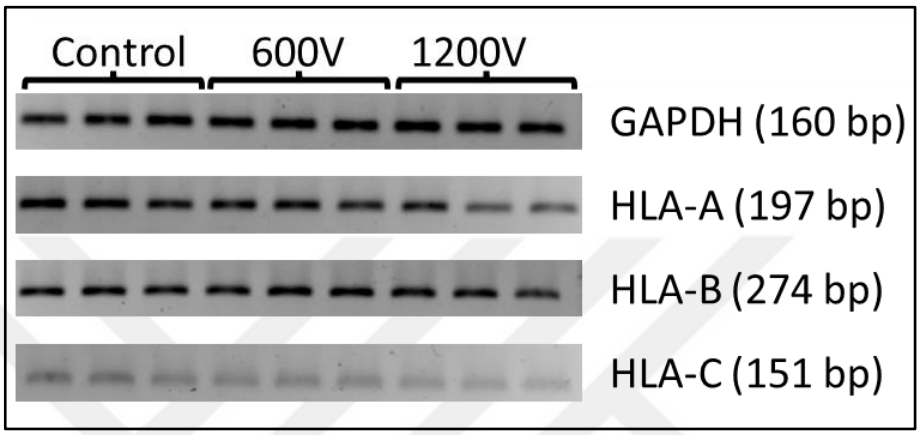

Figure 3. 12. Gel image of GAPDH, HLA- A, HLA- B, and HLA- C expressions of HDF cells 10 days after the application for 1 h with Control (0 V), 600 V, and 1200 V.

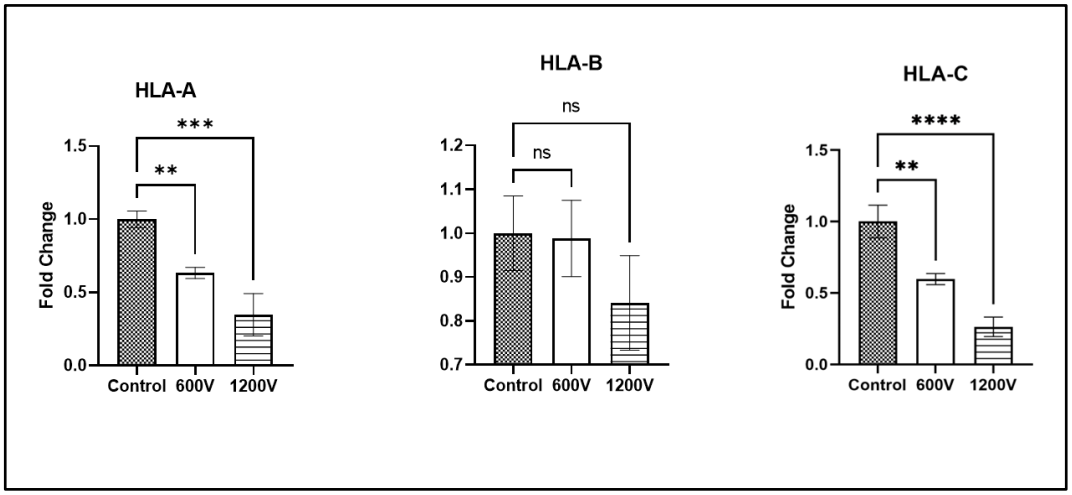

Figure 3. 13. Fold- change graphics of HLA- A, HLA- B, and HLA- C gene expression in HDF cells 10 days after 1 h EF application with 600 V and 1200 V electric sources. Gene expression normalization was performed using GAPDH as a housekeeping gene, and the overall fold change was normalized to Control group (0 V). A one- way ANOVA (Dunnett's multiple comparison test) was used to determine the significant difference in the fold change of the gene expressions: *p <0.05, **p<0.01, ***p<0.001 and, ****p< 0.0001 (n= 3 for each group).

HLA- A, HLA- B, and GCM2 expression decreased after both EF applications, as shown in Figures 3.14 and 3.15. After 600 V and 1200 V EF applications, HLA- A decreased to 0.85 ± 0.16 and 0.47 ± 0.16 folds; HLA- B decreased to 0.87 ± 0.14 and 0.35 ± 0.12 folds; and GCM2 decreased to 0.85 ± 0.12 and 0.46 ± 0.18 folds, respectively, when compared to the Control group (0 V). The graphics provide a clearer depiction of the HLA- C and PTH expressions in Pt cells after application. In both genes, increased expression was observed; HLA- C expression increased to 1.80 ± 059 and 2.09 ± 0.63 folds, and PTH expression increased to 1.30 ± 0.015 and 1.46 ± 0.29 folds after 600 V and 1200 V EF applications, respectively. The statistical data was obtained from the gel images with the assistance of ImageJ. HLA- A, HLA- B, and GCM2 expression decreased after both EF applications, as shown in Figures 3.14 and 3.15. After 600 V and 1200 V EF applications, HLA- A decreased to 0.85 ± 0.16 and 0.47 ± 0.16 folds; HLA- B decreased to 0.87 ± 0.137 and 0.35 ± 0.122 folds; and GCM2 decreased to 0.85 ± 0.123 and 0.46 ± 0.181 folds, respectively, when compared to the Control group (0 V). The graphics provide a clearer depiction of the HLA- C and PTH expressions in Pt cells after application. In both genes, increased expression was

observed; HLA- C expression increased to 1.80 ± 059 and 2.09 ± 0.634 folds, and PTH expression increased to 1.30 ± 0.01 and 1.46 ± 0.29 folds after 600 V and 1200 V EF applications, respectively. The statistical data was obtained from the gel images with the assistance of the ImageJ program.

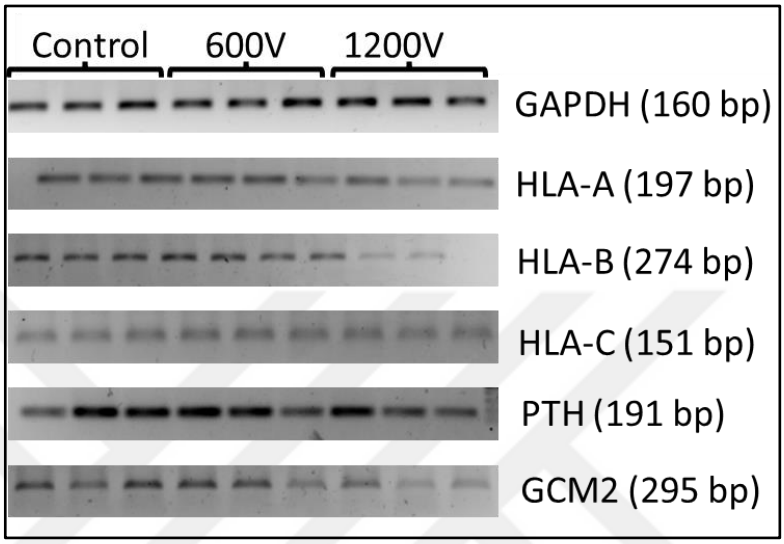

Figure 3. 14. Gel image of GAPDH, HLA- A, HLA- B, HLA- C, PTH, and GCM2 expressions of Pt cells 10 days after the EF application for 1 h with Control (0 V), 600 V, and 1200 V.

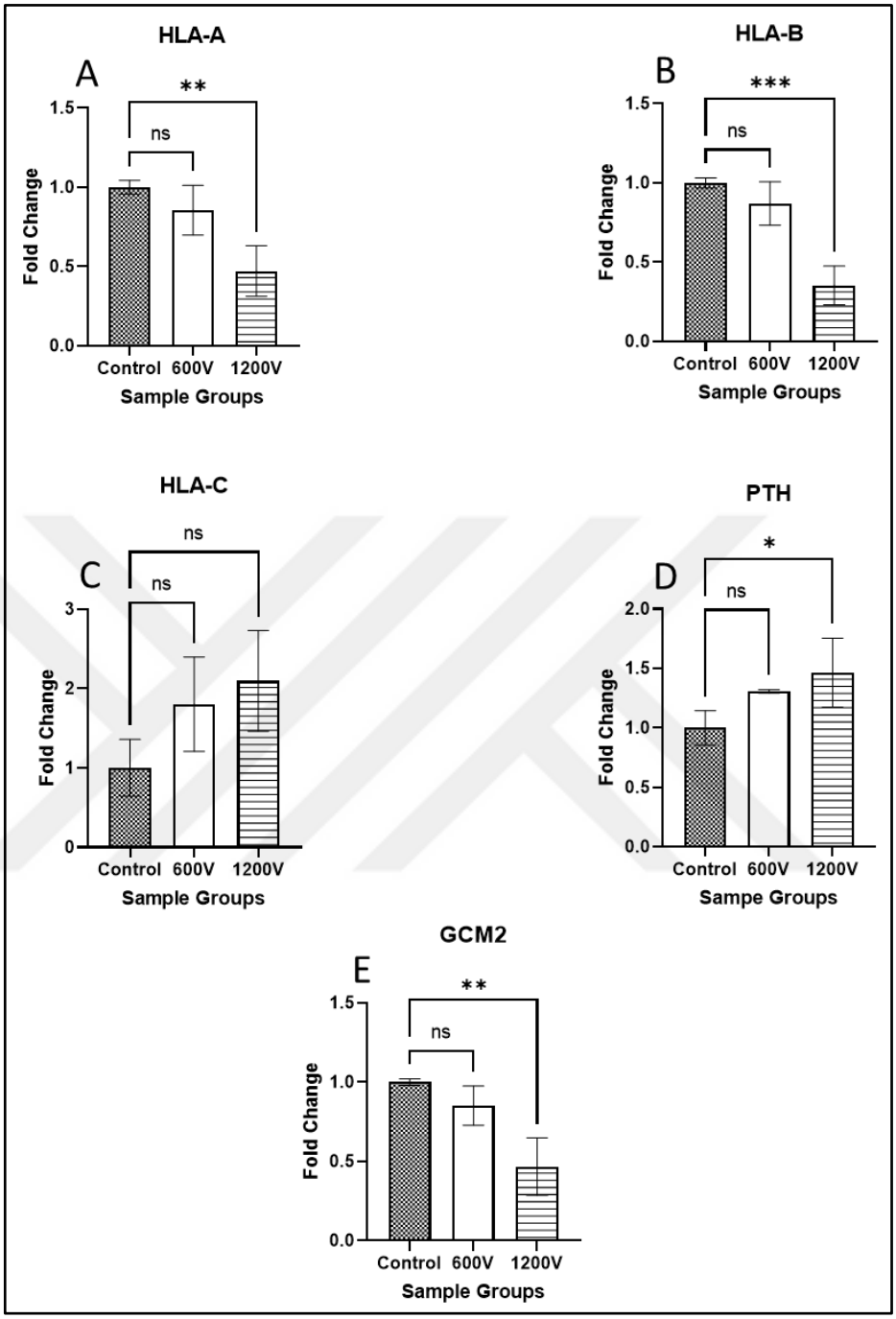

Figure 3. 15. Fold- change graphics of HLA- A, HLA- B, HLA- C, PTH, and GCM2 gene expression in Pt cells 10 days after 1 h EF application with 600 V and 1200 V electric sources. Gene expression normalization was performed using GAPDH as a housekeeping gene, and the overall fold change was normalized to Control groups (0 V). A one- way ANOVA (Dunnett's multiple comparison test) was used to determine the significant difference in the fold change of the gene expressions: *p <0.05, **p<0.01, ***p<0.001, and ****p< 0.0001 (n=3 for each group).

3.5. BIOCHEMICAL ANALYSIS

The biochemical analysis of PTH was performed by the Yeditepe Hospital Biochemistry Laboratory. The same volume of media was collected from all the Pt cell groups cumulatively, 20 h before and after EF treatment. PTH concentration results are shown in Table 3.3 and Figure 3.16.

The difference in concentration (pg/mL) of released PTH in the media 20 h before and after EF application was revealed by PTH biochemical analysis. Before EF application, PTH was detected as 687.3 ± 55.52 pg/mL in the Control (0 V), 719.3 ± 60.35 pg/mL in the 600 V, and 726.7 ± 28.43 pg/mL in the 1200 V groups, respectively. After EF application for 1 h, the test detected 1424.0 ± 153.87 pg/mL in the Control (0 V), 1689.3 ± 392.31 pg/mL in the 600 V, and 1329.0 ± 167.39 pg/mL in the 1200 V groups, respectively. Statistical analysis showed that there was no significant difference in the released PTH concentration when the Control (0 V) groups were compared with the 600 V and 1200 V groups, respectively. PTH concentrations increased significantly ($p < 0.01$) in the Control (0 V), and 1200 V groups 20 h after EF application when compared to 20 h before EF application. When PTH concentrations at 600 V were compared 20 h before and after EF application, they increased significantly ($p<0.001$).

Table 3. 3. PTH measurement (pg/mL) results from Pt cells 20 h before and after 1 h of EF application with 0 V, 600 V, and 1200 V (n=3 for each group).

Samples	**Control (0 V)**	**600 V**	**1200 V**
Before the EF application	687.3 ± 55.52 pg/mL	719.3 ± 60.35 pg/mL	726.7 ± 28.43 pg/mL
After the EF application	1424.0 ± 153.87 pg/mL	1689.3 ± 392.31 pg/mL	1329.0 ± 167.39 pg/mL

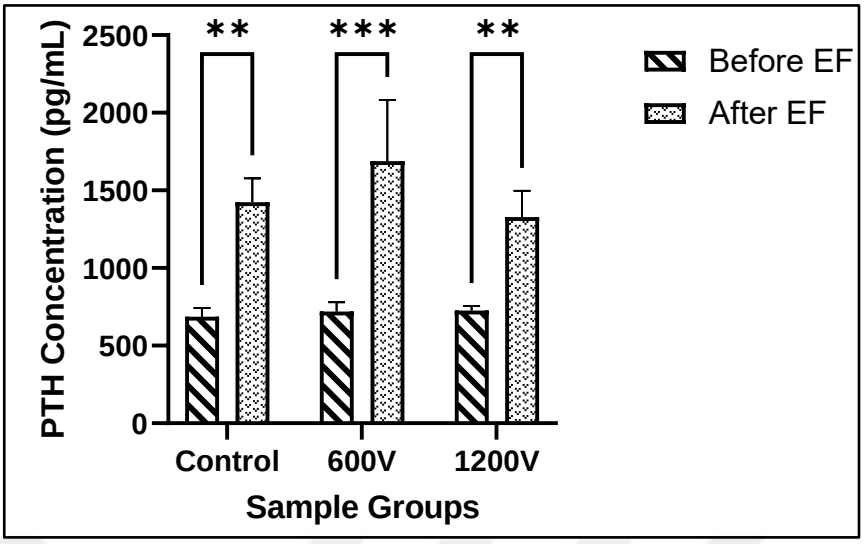

Figure 3. 16. Biochemical analysis of the media of Pt cells 20 h before and after 1 h of EF application with Control (0 V), 600 V, and 1200 V electric source. The comparison was applied according to both 20 h before and after EF application and according to Control (0 V) at 600 V and Control (0 V) at 1200 V. The one- way ANOVA (Šídák's multiple comparisons test) was used to determine the significant difference in PTH secretion for each comparison. *p <0.05, **p<0.01, ***p<0.001, and ****p< 0.0001 (n=3 for each group).

3.6. OXIDATIVE STRESS DETECTION

The effect of EF on ROS activation in Pt cells was determined by an oxidative stress detection assay. Samples were stained with CellROX™ Orange Reagent 1 h (Figure 3.17) and 20 h (Figure 3.18) after EF application. Samples were analysed using flow cytometry and the CytExpert software. As shown in Figure 3.17, the mean fluorescent intensity (MFI) of the samples 1 h after EF application was as follows: Control (0 V): 86.43 ± 15.29, 600 V: 66.03 ± 8.34, and 1200 V: 45.63 ± 5.60. There was a significant decrease ($p<0.001$) in ROS activity at 1200 V EF application. As shown in Figure 3.18, the MFI of the samples 20 h after EF application was as follows: Control (0 V): 107.33 ± 14.06, 600 V: 84.97 ± 3.97, and 1200 V: 81.13 ± 7.15. ROS activity decreased significantly ($p<0.05$) in both the 600 V and 1200 V EF applied groups.

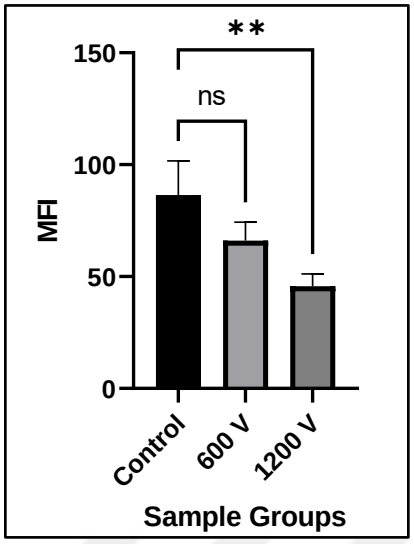

Figure 3. 17. Mean fluorescent intensity graphic of the oxidative stress detection assay after 1 h of EF application. To determine the significant difference in sample ROS activity, a one- way ANOVA (Dunnett's multiple comparison test) was used: *p<0.05, **p<0.01, ***p<0.001, and ****p<0.0001 (n = 3 for each group).

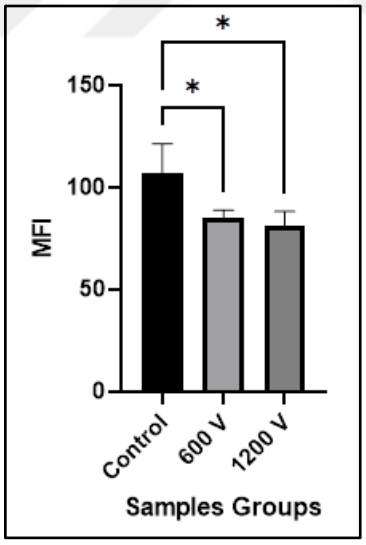

Figure 3. 18. Mean fluorescent intensity graphic of oxidative stress detection assay after 20 h of EF application. To determine the significant difference in sample ROS activity, a one-way ANOVA (Dunnett's multiple comparison test) was used: *p<0.05, **p<0.01, ***p<0.001, and ****p<0.0001 (n = 3 for each group).

3.7. CA^{2+} ION DETECTION ASSAY

To determine the possible effects of EF application on the calcium influx of Pt cells, the calcium concentration in the media was measured 1 and 20 h after EF application and calculated according to the standard curve (Figure 3.19). As shown in Figure 3.20, the media calcium concentration of the samples 1 h after EF application was as follows: Control (0 V): 2.44 mg/dL ± 0.69, 600 V: 3.16 mg/dL ± 0.86, and 1200 V: 3.35 mg/dL ± 1.03. As shown in Figure 3.21, the media calcium concentration of the samples 20 h after EF application is as follows: Control (0 V): 3.56 mg/dL ± 1.16, 600 V: 3.22 mg/dL ± 1.17, and 1200 V: 3.27 mg/dL ± 1.12. Neither of the EF- applied samples showed a significant change in the media Ca^{2+} levels after 1 and 20 h later of the respective applications.

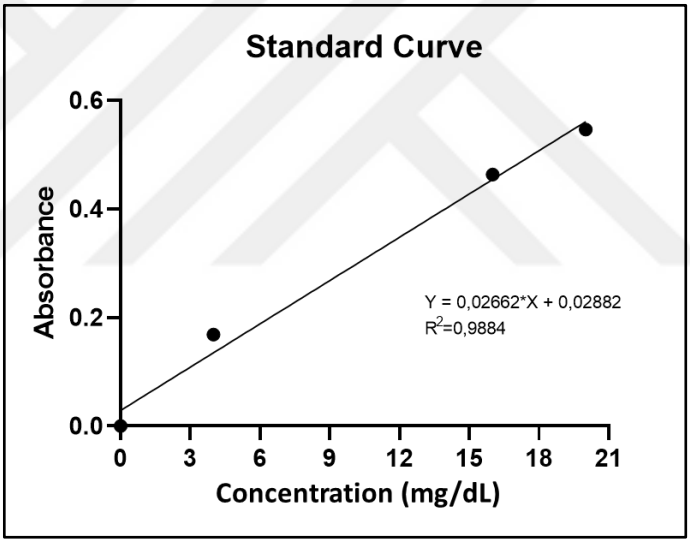

Figure 3. 19. Standard curve of Ca2+ concentration based on absorbance values of 0, 4, 16, and 20 mg/dL standard samples. The equation for the trendline is y = 0.02662*x + 0.02882; R^2 = 0.9884.

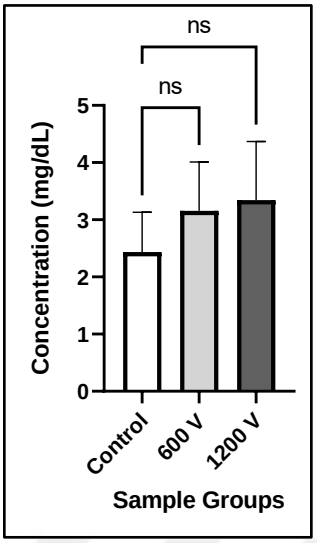

Figure 3. 20. Media calcium concentration graphic 1 h after EF application. To determine the significant difference in sample media calcium concentration, a one- way ANOVA (Dunnett's multiple comparison test) was used: *p<0.05, **p<0.01, ***p<0.001, and ****p<0.0001 (n = 3 for each group).

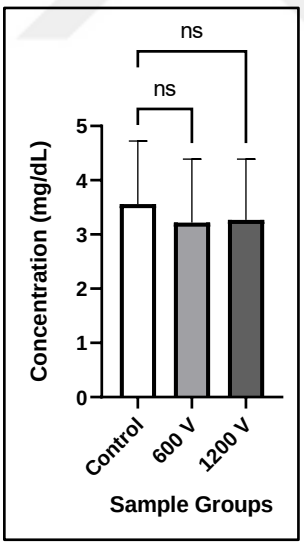

Figure 3. 21. Media calcium concentration graphic 20 h after EF application. To determine the significant difference in sample media calcium concentration, a one- way ANOVA (Dunnett's multiple comparison test) was used: *p<0.05, **p<0.01, ***p<0.001, and ****p<0.0001 (n = 3 for each group).

3.8. PH DETECTION

To determine the possible effects of EF on the pH level of media, media samples were collected, and measured with a pH meter. As depicted in Figure 3.22, the media pH level of the samples 1 h after EF application is as follows: Control (0 V): 8.57 ± 0.184, 600 V: 8.83 ± 0.279, and 1200 V: 8.58 ± 0.357. None of the EF- applied samples expressed a significant change in the media pH level 1 h after the respective applications. As shown in Figure 3.23, the media pH level of the samples 20 h after EF application is as follows: Control (0 V): 8.64 ± 0.327, 600 V: 9.38 ± 0.502, and 1200 V: 9.38 ± 0.491. Both 600 V and 1200 V EF- applied samples expressed a significant increase ($p<0.05$) in the media pH level 20 h after the respective applications.

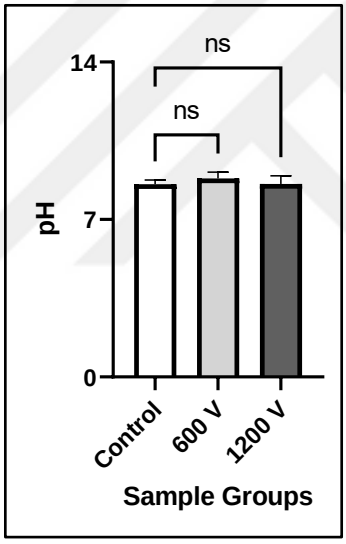

Figure 3. 22. Media pH graphic 1 h after EF application. To determine the significant difference in sample media pH, a one- way ANOVA (Dunnett's multiple comparison test) was used: *$p<0.05$, **$p<0.01$, ***$p<0.001$, and ****$p<0.0001$ (n = 3 for each group).

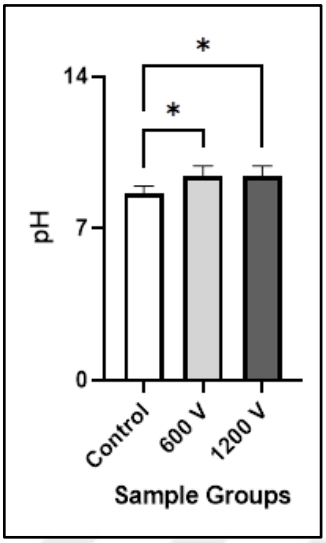

Figure 3. 23. Media pH graphic 20 h after EF application. To determine the significant difference in sample media pH, a one- way ANOVA (Dunnett's multiple comparison test) was used: *p<0.05, **p<0.01, ***p<0.001, and ****p<0.0001 (n = 3 for each group).

4. DISCUSSION

HypoPT is an endocrine system disorder caused by a lack of PTH; thus, treatments include protocols to reduce the severity of the symptoms through the use of calcium, vitamin D, and recombinant PTH supplements [37,38]. However, these supplements only provide short-term relief and can therefore be expensive for the patient. Pt allotransplantation is the unique and permanent treatment option for HypoPT. As in every other transplantation protocols, Pt allotransplantation may result in issues caused by the recipient's immune system. The host's immune system recognizes the transplant as an unknown material and attempts to eliminate it. This recognition is accomplished primarily by non- self HLA class I complexes on foreign cells and the TCR of recipient T lymphocytes [180]. Currently, immunosuppressive drugs are administered prior to and after transplantation to prevent rejection [42]. Despite the impressive effects of immunosuppressive drugs on transplant survival, they also suppress the recipient's immune system, resulting in a weakened defense against pathogens and cancerous cells in the early stages of development [41,42] and might cause hyperglycaemia, diabetes mellitus, oedema, hypertension, hyperlipidemia, hypokalaemia, hirsutism, arthralgia, osteoporosis, and psychosis [181].

Consequently, this study aims to develop a novel transplantation protocol, especially for Pt allotransplantation, so that immunosuppressive drugs are not needed as often or at all. To reach this goal, we focused our study on the main problem in transplant rejection: non- self HLA class I complexes to which the recipient's immune system reacts. Our research showed that the expression of classical HLA class I surface markers decreased when EFs were applied to cells. This may increase the transplant success rate.

Before determining the EF effect on cells, it was necessary to establish that the EFs did not compromise cell viability. In this instance, EFs were measured using HDF cells as a model cell line. Since HDF cells were easier to work with and were non- polar, they were an ideal model system to test the effects of the EF, compared to using the fragile and hard- to- acquire Pt cells. Between 100 V and 5000 V, HDF cell viability, shape, and multiplication ability did not deteriorate. Within this range, 600 V and 1200 V induced the greatest differences in the expression of key genes for immune reactions, such as HLA- A, HLA- B, and HLA- C.

Therefore, these voltages were used in future studies. Expression of several housekeeping genes, such as 18SRNA and β- actin, was affected by the EF application. GAPDH was found to be unaffected by EF and therefore was used to normalize the gene expressions of the desired classical HLA class I isoforms, PTH, and GCM2. Even though GAPDH gene expression differs between Pt and HDF cells, GAPDH gene expression did not undergo the drastic alteration observed in both β- actin and 18SRNA expressions.

The viability of Pt and HDF cells was assessed using an Annexin- V and PI assay 24 h after application and a Live/Dead viability assay 48 and 72 h later. After 24 h, EF applied at 600 V and 1200 V significantly increased HDF cell viability. Due to the shorter doubling time of HDF cells compared to Pt cells, the effect of EF might have been eliminated from HDF cells in a shorter time frame. So, the potential permeabilizing effect of EF could return to normal 24 h after its application. This recovery could prevent both the apoptotic dye Annexin- V and the necrotic dye PI from penetrating the cell for analysis. On the other hand, a shorter doubling time might have caused a significant increase in cell viability. It is known that EF can increase proliferation in various cell types. Banks *et al.* found that the EF effect caused changes in cellular behaviour, such as increased proliferation in human mesenchymal stem cells, which Kumar *et al.* demonstrated in osteoblast cells as well [161,165]. Furthermore, the Live/Dead viability assay results revealed no difference in viable HDF cell populations between the Control (0 V), 600 V, and 1200 V groups after 48 h and 72 h, as indicated by the green fluorescent signal. Since HDF cells have a shorter doubling time, as expected, the cell population observed in 72 h samples was much denser than in 48 h samples.

According to the data, 1 h of EF application slightly affected the viability of Pt cells 24 h after the application. However, since this high- magnitude EF is also used for permeabilization procedures [166], the high number of late- apoptotic cells might be due to the permeabilization of the cell membrane. Both Annexin- V and PI dyes are dependent on the integrity of the cell membrane, and if the cell membrane of Pt cells were permeabilized, this would explain the presence of many late- apoptotic cells, indicated as double- positive signals in flow cytometry. Since the doubling time of Pt cells is longer than that of HDF cells, this could explain why HDF cells did not experience this problem. The results obtained from the 48 h and 72 h Live/Dead viability assay samples also supported this hypothesis. If

cell viability decreased 24 h after EF application, we would anticipate a greater number of dead cells in the fluorescent microscopy images at 48 h and 72 h. However, in both 600 V and 1200 V EF- applied Pt cell samples, there were very few red fluorescently labeled dead cells, and there was no difference in the number of living and dead cells compared to the Control (0 V) groups.

One of the main aims of this project was to determine whether the EF influences the expression of the classical HLA class I gene. To investigate this hypothesis, PCR and gel electrophoresis techniques were utilized. The application of EF to HDF cells, regardless of the magnitude of the source, decreased HLA isoform gene expression, and it was also associated with a significant decrease in HLA- A and HLA- C expressions.

On the other hand, gene expression alterations in Pt cells after EF application with 600 V and 1200 V sources diverged. Even though the 600 V source showed a decrease in isoforms of the classical HLA class I protein genes HLA- A, HLA- B, and GCM2, the difference was not statistically significant for any of the studied genes. Gene expressions of HLA- C and PTH increased, though insignificantly. The gene expression levels of HLA- A, HLA- B, and GCM2 decreased significantly after a 1200 V- sourced EF was applied. Similar to 600 V samples, 1200 V samples exhibited an increase in both HLA- C and PTH gene expressions, yet only the increasing fold- change in PTH was statistically significant.

Changes in gene expression could be observed due to intracellular and transmembrane charge alterations induced by EF application. Considering that all interactions between protein complexes depend on electrical charges, modifying the electrical charges may affect gene expression through proteins such as histone proteins or transcription factors. The findings of Li *et al.*, showed that applying EF could change the methylation of DNA. Thus, gene expression may differ [158]. Sheikh *et al.*, on the other hand, proposed that low-amplitude EF could influence the regulation of some of the main functional pathways, such as the MAPK/ERK pathway [182]. Any change in the electrical charges of one or more of these structures could alter total gene expression. Since each of the examined genes are located in a distinct region of the genome, even though the classical HLA class I genes is in

close proximity, the application of EF could affect the expressions differently, either directly or indirectly.

Changes in protein and gene expressions are not always correlated. Regardless of gene expression alterations, neither the Control (0 V) nor the EF applied groups expressed a complete understanding of HDF and Pt cell protein expressions. In the case of decreasing gene expressions of HLA- A and HLA- B in HDF and HLA- A and HLA- C in Pt cells, all statements regarding protein expressions would be speculative. The expression of proteins within the cell and on the cell membrane could be changed by EF application. Application of EF may also alter the half- life of mRNAs and protein complexes, resulting in increased protein expression even when gene expression is low [183]. On the other hand, increased HLA- B expression in HDF and HLA- C expression in Pt may have the opposite effect [184,185]. Increased gene expressions may not necessarily correlate with increased protein expression in cells.

Biochemical analysis showed a significant increase in PTH secretion in each group when compared to the same samples collected 20 h before and after EF application. Since increasing PTH gene expression was observed, it was anticipated that PTH secretion would also increase in 600 V and 1200 V EF- applied samples after respective applications. The increased PTH secretion in the Control (0 V) group was an unexpected result. There might be multiple possible causes for this issue. First of all, both Control (0 V) and EF- applied samples were placed in the same incubator during the application process. EF is not a force that could be isolated, so even though there was a non- conducting plate between the aluminium plates and the incubator shelf, Control (0 V) groups could still be affected by the minimal EF. Despite the effect of EF, the Control (0 V) group was not affected to the same extent as the 600 V and 1200 V groups. However, it is well known in the literature that minimal EF could affect cells in a variety of ways, including increased proliferation [161,165,186,187], altered secretion [175], and functional alterations [156,158,164,182,188]. If the Control (0 V) groups were affected by this minimal EF, their proliferation and, as a result, PTH secretion could have increased. Secondly, minimal EF may have altered the ion homeostasis [189] of the Control (0 V) groups, which might have triggered PTH secretion. Thirdly, the minor effect of EF may have altered the functional pathways of PTH production and secretion, leading to increased secretion. In the case of 600

V and 1200 V EF- applied samples, there was a significant difference between 20 h before and after the EF applications. However, there was no significant difference in either group 20 h after the application when compared to the Control (0 V) group. Even though the fold-change in PTH gene expression was significantly increased, PTH secretion in the same samples did not increase significantly. This could be due to the altered half- life of the PTH protein and/or the affected molecular pathway of PTH production and secretion as a result of EF. However, these findings showed that EF application with either voltage source had no undesired effect on PTH secretion.

Reactive oxygen species are produced due to metabolic activities such as mitochondrial activity, cellular responses to cytokines, and bacterial infection. Oxidative stress occurs due to an imbalance between the cellular capacity of the antioxidant response and the ROS generated within the cell. Either a decrease in the antioxidative response or an increase in ROS generation causes this [191]. This oxidative stress is directly or indirectly related to nucleic acid damage, lipids, and proteins that are linked with neurodegeneration [191,192], carcinogenesis [193], diabetes [191,192], atherosclerosis, and aging [194]. The effect of EF on ROS activity depends on the strength of the EF. ROS activity increased in the case of nsPEF at 5, 10, and 20 kV/cm; however, at 5 kV/cm, nsPEF was the highest ROS activity sample, and 20 kV/cm was the lowest of these three different EF sources [196]. A study in 2018 demonstrated that ROS activity begins to increase 1 h after PEF with 120 kV/cm compared to right after PEF application [196]. In another study, ROS activity increased from 0 to 3 h after 3 MV/m EF application.

In this project, the generation of ROS 1 and 20 h after EF application was determined by an oxidative stress detection protocol. When 1200 V EF application to Pt cells was compared with the Control group (0 V), ROS activity decreased significantly ($p<0.001$) 1 h after EF application. Similarly, cells showed a significant decrease ($p<0.05$) in ROS activity 20 h after EF application. In 600 V EF- applied groups, EF application had no significant effect on cells after 1 h; however, 20 h after 600 V EF application, ROS activity decreased significantly ($p<0.05$). According to the literature, the effect of EF on ROS activity varies under different conditions; for example, there are instances in which the first time interval has less ROS activity than the second- chosen time interval [196,197]. Application of the EF might have permeabilized the cell membrane, causing an influx of ROS outside the cell,

resulting in the ROS activity determined by the oxidative stress detection assay to be significantly less compared to the Control group (0 V) in 1 h after 1200 V EF application. According to the results, the effect of EF on ROS activity should be investigated further.

To determine the possible effects of EF on the calcium metabolism of Pt cells, a calcium detection assay was performed on the media of the cells. According to Khatib *et al.*, EF applications can induce an increase in cytosolic Ca^{2+} concentration, but it is not an immediate reaction. They showed that the Ca^{2+} concentration in the cells is affected by EF applications differently depending on the intensity of the EF and the duration of the application. Additionally, they also demonstrated that EF induces Ca^{2+} influx from the media and from intracellular Ca^{2+} stores, thereby increasing cytosolic Ca^{2+} concentration [198,199]. Application of EF strong enough to act as a depolarizing agent for the cell membrane could induce voltage- gated Ca^{2+} channels (VGCC) on the membrane to induce Ca^{2+} influx [200]. Our results showed that 600 and 1200 V EF applications to Pt cells did not induce a significant change in Ca^{2+} concentration 1 h after the application. Even though the change was not statistically significant, there was a slight decrease in media Ca^{2+} concentration 20 h after EF application. This data correlated with our findings regarding PTH secretion 20 h after EF application. PTH secretion increased insignificantly 20 h after EF application in both 600 and 1200 V sample groups. Since PTH secretion is directly related to the Ca^{2+} concentration in the environment, an insignificant decrease in Ca^{2+} might have triggered PTH secretion. Despite the fact that the results are insignificant, the slight alterations in the results suggest a promising outcome if the effect of the EF application on Ca^{2+} concentration is further investigated.

Using a pH meter, the EF effect on the pH level of the Pt cell media was determined. Since Pt cells demonstrated changes in their Ca^{2+} concentration, gene expressions, PTH secretions, and ROS activity, these alterations could induce a pH level change in the media. Ca^{2+} influx may have caused a concentration change in the media, resulting in a Na^{+} concentration that induced an alkaline media pH. pH levels were increased in both media collected after 1 and 20 h, even though only the 20- h samples showed a statistically significant result ($p<0.05$).

5. CONCLUSION

Pt transplantation offers a unique and permanent treatment option for HypoPT patients, but immune activation related graft rejection is a common issue in this procedure. In this study, we investigated the potential effects of EF on Pt cells that affect the classical HLA class I molecules and thus, increase the survival rate of the transplanted Pt cells. This study suggests that pre- transplantation EF treatment of Pt cells may be an effective way to reduce the likelihood of an immune response after transplantation. The results showed that 600 V or 1200 V EF applications had no effect on the viability of Pt cells. On the other hand, 1200 V-sourced EF significantly reduced HLA- A and HLA- B gene expressions and significantly increased PTH gene expression. ROS activity of 600 V and 1200 V EF - applied samples showed that 1 h after EF application, ROS activity in Pt cells decreased significantly. These findings suggest that applying EF, particularly 1200 V- sourced EF, can be used as an alternative to immunosuppressive drugs to eliminate and/or reduce immune activation following transplantation.

6. FUTURE ASPECTS

The main purpose of this study was to investigate the potential effects of EF on Pt cell viability and gene expression. Even though our results are encouraging for the future of Pt transplantation without the need for immunosuppressive drugs, there are still a few aspects of this study that require additional investigation. Because immune activation following transplantation is based on protein expression on the surface of the cells, a protein analysis such as a western blot could be useful for answering questions regarding the potential decrease in immune activation following transplantation. The western blot technique could also be useful for the determination of PTH secretion from Pt cells. The findings in this study suggested a new questions about the proliferation of Pt cells, ROS activity following EF application, and changes in Ca^{2+} influx. A proliferation assay performed before and after the EF application could reveal the effect of EF on cell proliferation. Further investigations on ROS activity, such as the levels of antioxidant enzymes and the levels of ROS activity after both EF application and treatment with an oxidative reagent, could have promising outcomes. An investigation of calcium metabolism by blocking either transmembrane or intercellular calcium gates could suggest a promising result in the effect of EF on the Ca^{2+} influx and PTH secretion patterns of Pt cells since these two mechanisms are closely related. Before proceeding with *in vivo* and clinical trials, any possible effects of EF on undesirable functional and genetic outcomes, such as the potential activity of protooncogenes, should be eliminated. Proteomic and genomic analysis for different protein and/or gene expressions after EF application could also be helpful to demonstrate that EF application has little to no undesired effects and thus induces desired effects such as reducing HLA gene and protein expression on Pt cells. In this project, the effect of EF on HLA class I gene expression was determined 10 days after the application. Experimentation with longer time points could suggest a better understanding of the possible permanent effect of EF on gene and protein expression in Pt cells. EF-applied cells and activated T cells might be co-cultured to determine the possible change in the immune activity capacity of Pt cells after EF application. Even with these possible *in vitro* experiments, further *in vivo* testing is still required. If both *in vivo* and *in vitro* tests correlate with our results, EF applications could be beneficial for transplantation procedures to reduce immune activation after transplantation permanently.

REFERENCES

1. Fancy T, Gallagher D, Hornig JD. Surgical anatomy of the thyroid and parathyroid glands. *Otolaryngol Clin North Am*. 2010;43(2):221–7.

2. Åkerström G, Malmaeus J, Bergström R. Surgical anatomy of human parathyroid glands. *Surgery*. 1984;95(1):14–21.

3. Arrangoiz R, Ridge JA. Parathyroid Carcinoma. *Textb Uncommon Cancer*. 2012;201–9.

4. Gomes EMDS, Nunes RC, Lacativa PGS, De Almeida MH, Franco FM, Leal CTS, et al. Ectopic and extranumerary parathyroid glands location in patients with hyperparathyroidism secondary to end stage renal disease. *Acta Cir Bras*. 2007;22(2):105–9.

5. Casale J, Giwa AO. Embryology, Branchial Arches. In: StatPearls [Internet]. Treasure Island (FL): StatPearls Publishing; 2019.

6. Peissig K, Condie BG, Manley NR. Embryology of the parathyroid glands. *Endocrinol Metab Clin North Am*. 2018;47(4):733.

7. Frisdal A, Trainor PA. Development and Evolution of the Pharyngeal Apparatus. *Wiley Interdiscip Rev Dev Biol*. 2014;3(6):403.

8. Grevellec A, Tucker AS. The pharyngeal pouches and clefts: Development, evolution, structure and derivatives. *Semin Cell Dev Biol*. 2010;21(3):325–32.

9. LoPinto M, Rubio GA, Khan ZF, Vaghaiwalla TM, Farra JC, Lew JI. Location of abnormal parathyroid glands: lessons from 810 parathyroidectomies. *J Surg Res*. 2017;207:22–6.

10. Phitayakorn R, McHenry CR. Incidence and location of ectopic abnormal parathyroid glands. *Am J Surg*. 2006;191(3):418–23.

11. Uno N, Tominaga Y, Matsuoka S, Tsuzuki T, Shimabukuro S, Sato T, et al. Incidence of parathyroid glands located in thymus in patients with renal hyperparathyroidism. *World J Surg*. 2008;32(11):2516–9.

12. Arrangoiz R, Cordera F, Caba D, Juárez MM, Moreno E, Luque E, et al. Parathyroid Embryology, Anatomy, and Pathophysiology of Primary Hyperparathyroidism. *Int J Otolaryngol Head & Neck Surg*. 2017;6(4):39–58.

13. Policeni BA, Smoker WRK, Reede DL. Anatomy and embryology of the thyroid and parathyroid glands. *Semin Ultrasound CT MR*. 2012;33(2):104–14.

14. Chen RA, Goodman WG. Role of the calcium-sensing receptor in parathyroid gland physiology. *Am J Physiol Renal Physiol*. 2004;286(6):F1005–11.

15. Wardle EN, Kurihara I, Saito T, Obara K, Shoji Y, Hirai M, et al. Oxyphil Cell Function in Secondary Parathyroid Hyperplasia. *Nephron*. 1996;73(4):580–6.

16. Christie AC. The parathyroid oxyphil cells. *J Clin Pathol*. 1967;20(4):591–602.

17. Ritter CS, Haughey BH, Miller B, Brown AJ. Differential Gene Expression by Oxyphil and Chief Cells of Human Parathyroid Glands. *J Clin Endocrinol Metab*. 2012;97(8):E1499.

18. Nonaka D. Study of parathyroid transcription factor Gcm2 expression in parathyroid lesions. *Am J Surg Pathol*. 2011;35(1):145–51.

19. Vilardaga J-P, Friedman PA. Molecular Biology of Parathyroid Hormone. In: Textbook of Nephro-Endocrinology. Academic Press; 2018. p. 523–37.

20. Beunter EH, Munson PL. Time course of urinary excretion of inorganic phosphate by rats after parathyroidectomy and after injection of parathyroid extract. *Endocrinolgy*. 1960;66:610–6.

21. Pullman T, Lavender, ARAho I. Direct renal action of a purified parathyroid extract. *Endocrinolgy*. 1960;67.

22. Greenwald I, Gross J. The effect of the administration of a potent parathyroid extract upon the excretion of nitrogen, phosphorus, calcium, and magnesium, with some remarks on. *J Biol Chem*. 1925;66:217–27.

23. Munson PL. Studies on the role of parathyroids in calcium and phosphorus metabolism. *Ann N Y Acad Sci*. 1955;60(5):776–96.

24. Bingham P, Brazell I, Owen M. The effect of parathyroid extract on cellular activity and plasma calcium levels in vivo. *J Endocrinol*. 1969;45(3):387–400.

25. CHANG HY. Grafts of parathyroid and other tissues to bone. *Anat Rec*. 1951;111(1):23–47.

26. Barnicot N. The local action of the parathyroid and other tissues on bone in intracerebral grafts. *J Anat*. 1948;82(Pt4):233–48.

27. Fraser D, Kodicek E. Regulation of 25-hydroxycholecalciferol-1-hydroxylase activity in kidney by parathyroid hormone. *Nat New Biol*. 1973;241:163–6.

28. Garabedian M, Holick MF, Deluca HF, Boyle IT. Control of 25-hydroxycholecalciferol metabolism by parathyroid glands. *Proc Natl Acad Sci U S A*. 1972;69(7):1673–6.

29. Talmage R V., Kraintz FW. Progressive Changes in Renal Phosphate and Calcium Excretion in Rats Following Parathyroidectomy or Parathyroid Administration. *Proc Soc Exp Biol Med*. 1954;87(2):263–7.

30. Lee M, Partridge NC. Parathyroid hormone signaling in bone and kidney. *Curr Opin Nephrol Hypertens*. 2009;18(4):298–302.

31. Khan M, Jose A, Sharma S. Physiology, Parathyroid Hormone. In: StatPearls [Internet]. Treasure Island (FL): StatPearls Publishing; 2021.

32. Sugarman J, Douglass A, Say EA, Shields C. Stones, bones, groans, thrones, and psychiatric overtones: Systemic associations of sclerochoroidal calcification. *Oman J Ophthalmol*. 2017;10(1):47–9.

33. Pitt SC, Sippel RS, Chen H. Secondary and Tertiary Hyperparathyroidism, State of the Art Surgical Management. *Surg Clin North Am*. 2009;89(5):1227–38.

34. Walker MD, Silverberg SJ. Primary hyperparathyroidism. *Nat Rev Endocrinol*. 2018;14(2):115–25.

35. Kraus C, Vanicek T, Weidenauer A, Khanaqa T, Stamenkovic M, Lanzenberger R, et al. DiGeorge syndrome : Relevance of psychiatric symptoms in undiagnosed adult patients. *Wien Klin Wochenschr*. 2018;130(7–8):283–7.

36. Forsmark C, Pham A. Chronic pancreatitis: Review and update of etiology, risk factors, and management. *F1000Research*. 2018;7:1–11.

37. Bilezikian JP, Brandi ML, Cusano NE, Mannstadt M, Rejnmark L, Rizzoli R, et al. Management of Hypoparathyroidism: Present and Future. *J Clin Endocrinol Metab*. 2016;101(6):2313–24.

38. Aysan E, Kilic U, Gok O, Altug B, Ercan C, Toka CK, et al. Parathyroid allotransplant for persistent hypocalcaemia: A new technique involving short-term culture. *Exp Clin Transplant*. 2016;14(2):238–41.

39. Barczyński M, Golkowski F, Nawrot I. Parathyroid transplantation in thyroid surgery. *Gland Surg*. 2017;6(5):530–6.

40. Bjerneroth G, Juhlin C, Rastad J, ÅKerstrÖM Gör, Klareskog L. MHC class I and II antigen expression on parathyroid cells and prospects for their allogenic transplantation. *Transplantation*. 1993;56(3):717–21.

41. Gallagher MP, Kelly PJ, Jardine M, Perkovic V, Cass A, Craig JC, et al. Long-Term Cancer Risk of Immunosuppressive Regimens after Kidney Transplantation. *J Am Soc Nephrol*. 2010;21(5):852–8.

42. Duncan MD, Wilkes DS. Transplant-related Immunosuppression: A Review of Immunosuppression and Pulmonary Infections. *Proc Am Thorac Soc*. 2005;2(5):449–55.

43. Goncu B, Yucesan E. Microencapsulation for Clinical Applications and Transplantation by Using Different Alginates. In: Abu-Thabit N, editor. Nano- and Microencapsulation - Techniques and Applications. 1st ed. IntechOpen; 2020. p. 1–12.

44. Chandy T, Mooradian DL, Rao GHR. Evaluation of modified alginate-chitosan-polyethylene glycol microcapsules for cell encapsulation. *Artif Organs*. 1999;23(10):894–903.

45. Lee CH, Singla A, Lee Y. Biomedical applications of collagen. *Int J Pharm*. 2001;221(1–2):1–22.

46. Miyamoto T, Takahashi S -i, Ito H, Inagaki H, Noishiki Y. Tissue biocompatibility of cellulose and its derivatives. *J Biomed Mater Res*. 1989;23(1):125–33.

47. Iwata H, Amemiya H, Matsuda T, Takano H, Hayashi R, Akutsu T. Evaluation of microencapsulated islets in agarose gel as bioartificial pancreas by studies of hormone secretion in culture and by xenotransplantation. *Diabetes*. 1989;38 Suppl 1(SUPPL. 1):224–5.

48. Yucesan E, Basoglu H, Goncu B, Akbas F, Ersoy YE, Aysan E. Microencapsulated parathyroid allotransplantation in the omental tissue. *Artif Organs*. 2019;43(10):1022–7.

49. Felix NJ, Allen PM. Specificity of T-cell alloreactivity. *Nat Rev Immunol*. 2007;7(12):942–53.

50. Marino J, Paster J, Benichou G. Allorecognition by T lymphocytes and allograft rejection. *Front Immunol*. 2016;7(DEC):1–9.

51. Oberbarnscheidt MH, Zecher D, Lakkis FG. The innate immune system in transplantation. *Semin Immunol*. 2011;23(4):264–72.

52. Suchin EJ, Langmuir PB, Palmer E, Sayegh MH, Wells AD, Turka LA. Quantifying the frequency of alloreactive T cells in vivo: new answers to an old question. *J Immunol*. 2001;166(2):973–81.

53. Lindahl KF, Wilson DB. Histocompatibility antigen-activated cytotoxic T lymphocytes. II. Estimates of the frequency and specificity of precursors. *J Exp Med*. 1977;145(3):508–22.

54. Bevan MJ. High determinant density may explain the phenomenon of alloreactivity. *Immunol Today*. 1984;5(5):128–30.

55. Matzinger P, Bevan MJ. Hypothesis: why do so many lymphocytes respond to major histocompatibility antigens? *Cell Immunol*. 1977;29(1):1–5.

56. Flaherty DKBT-I for P, editor. Chapter 17 - Transplantation. In: Immunology for Pharmacy. Saint Louis: Mosby; 2012. p. 138–46.

57. Colvin RB. Antibody-mediated renal allograft rejection: diagnosis and pathogenesis.

J Am Soc Nephrol. 2007;18(4):1046–56.

58. Lachmann N, Terasaki PI, Budde K, Liefeldt L, Kahl A, Reinke P, et al. Anti-human leukocyte antigen and donor-specific antibodies detected by luminex posttransplant serve as biomarkers for chronic rejection of renal allografts. *Transplantation*. 2009;87(10):1505–13.

59. Wiebe C, Gibson IW, Blydt-Hansen TD, Karpinski M, Ho J, Storsley LJ, et al. Evolution and clinical pathologic correlations of de novo donor-specific HLA antibody post kidney transplant. *Am J Transplant*. 2012;12(5):1157–67.

60. Chesneau M, Michel L, Degauque N, Brouard S. Regulatory B cells and tolerance in transplantation: from animal models to human. *Front Immunol*. 2013;4(DEC):1–8.

61. Newell KA, Asare A, Kirk AD, Gisler TD, Bourcier K, Suthanthiran M, et al. Identification of a B cell signature associated with renal transplant tolerance in humans. *J Clin Invest*. 2010;120(6):1836.

62. Sagoo P, Perucha E, Sawitzki B, Tomiuk S, Stephens DA, Miqueu P, et al. Development of a cross-platform biomarker signature to detect renal transplant tolerance in humans. *J Clin Invest*. 2010;120(6):1848.

63. Cherukuri A, Rothstein DM, Clark B, Carter CR, Davison A, Hernandez-Fuentes M, et al. Immunologic human renal allograft injury associates with an altered IL-10/TNF-α expression ratio in regulatory B cells. *J Am Soc Nephrol*. 2014;25(7):1575–85.

64. Nouël A, Ségalen I, Jamin C, Doucet L, Caillard S, Renaudineau Y, et al. B cells display an abnormal distribution and an impaired suppressive function in patients with chronic antibody-mediated rejection. *Kidney Int*. 2014;85(3):590–9.

65. Shiu KY, Mclaughlin L, Rebollo-Mesa I, Zhao J, Semik V, Cook HT, et al. B-lymphocytes support and regulate indirect T-cell alloreactivity in individual patients with chronic antibody-mediated rejection. *Kidney Int*. 2015;88(3):560–8.

66. Stites E, Quintrec M Le, Thurman JM. The Complement System and Antibody Mediated Transplant Rejection. *J Immunol*. 2015;195(12):5525–31.

67. Della-Guardia B, Almeida MD, Meira-Filho SP, Torres MA, Venco F, Afonso RC, et

al. Antibody-Mediated Rejection: Hyperacute Rejection Reality in Liver Transplantation? A Case Report. *Transplant Proc*. 2008;40(3):870–1.

68. Shaik I, Carmody IC, Chen PW. Treatment of Acute and Chronic Rejection. In: Transplantation of the Liver: Third Edition. W.B. Saunders; 2015. p. 1317–28.

69. Novotny M, Hruba P, Kment M, Voska L, Kabrtova K, Slavcev A, et al. Intimal Arteritis and Microvascular Inflammation Are Associated With Inferior Kidney Graft Outcome, Regardless of Donor-Specific Antibodies. *Front Med*. 2021;8:1–10.

70. Hubscher SG, Buckels JAC, Elias E, McMaster P, Neuberger J. Vanishing bile-duct syndrome following liver transplantation-is it reversible? *Transplantation*. 1991;51(5):1004–10.

71. Lai X, Zheng X, Mathew JM, Gallon L, Leventhal JR, Zhang ZJ. Tackling Chronic Kidney Transplant Rejection: Challenges and Promises. *Front Immunol*. 2021;12:1–13.

72. Costello JP, Mohanakumar T, Nath DS. Mechanisms of Chronic Cardiac Allograft Rejection. *Texas Hear Inst J*. 2013;40(4):395–9.

73. Gorer PA, Lyman S, Snell GD, Haldane JBS. Studies on the genetic and antigenic basis of tumour transplantation Linkage between a histocompatibility gene and "fused" in mice. *Proc R Soc London Ser B - Biol Sci*. 1948;135(881):499–505.

74. Snell GD, Cherry M, Démant P. Evidence that H-2 private specificities can be arranged in two mutually exclusive systems possibly homologous with two subsystems of HL-A. *Transplant Proc*. 1971;3(1):183–6.

75. Thorsby E, Thorsby E. A short history of HLA. *Tissue Antigens*. 2009;74(2):101–16.

76. Payne R, Rolfs MR. Fetomaternal Leukocyte Incompatibility. *J Clin Invest*. 1958;37(12):1756–63.

77. Dausset J. Iso-leuko-antibodies. *Acta Haematol*. 1958;20(1–4):156–66.

78. Van Rood JJ, Eernisse JG, Van Leeuwen A. Leucocyte antibodies in sera from pregnant women. *Nature*. 1958;181(4625):1735–6.

79. J D, JP S. An interview with Jean Dausset. *Am J Transplant*. 2004;4(1):4–7.

80. Rajalingam R, Zhang Q, Cecka JM, Reed EF. Major Histocompatibility Complex. In: Li XC, Jevnikar AM, editors. Transplant Immunology. 1st ed. Wiley Blackwell; 2016. p. 126–47.

81. Hughes AL, Ota T, Nei M. Positive Darwinian selection promotes charge profile diversity in the antigen-binding cleft of class I major-histocompatibility-complex molecules. *Mol Biol Evol*. 1990;7(6):515–24.

82. Reche PA, Reinherz EL. Sequence Variability Analysis of Human Class I and Class II MHC Molecules: Functional and Structural Correlates of Amino Acid Polymorphisms. *J Mol Biol*. 2003;331(3):623–41.

83. Yeager M, Hughes AL. Evolution of the mammalian MHC: natural selection, recombination, and convergent evolution. *Immunol Rev*. 1999;167:45–58.

84. Knapp LA. The ABCs of MHC. *Evol Anthropol Issues, News, Rev*. 2005;14(1):28–37.

85. Lawlor DA, Ward FE, Ennis PD, Jackson AP, Parham P. HLA-A and B polymorphisms predate the divergence of humans and chimpanzees. *Nature*. 1988;335(6187):268–71.

86. Zangenberg G, Huang MM, Arnheim N, Erlich H. New HLA-DPB1 alleles generated by interallelic gene conversion detected by analysis of sperm. *Nat Genet*. 1995;10(4):407–14.

87. Hughes AL, Hughes MK, Watkins DI. Contrasting roles of interallelic recombination at the HLA-A and HLA-B loci. *Genetics*. 1993;133(3):669–80.

88. Stern LJ, Wiley DC. Antigenic peptide binding by class I and class II histocompatibility proteins. *Structure*. 1994;2(4):245–51.

89. Madden DR. The three-dimensional structure of peptide-MHC complexes. *Annu Rev Immunol*. 1995;13:587–622.

90. Braud VM, Allan DS, McMichael AJ. Functions of nonclassical MHC and non-MHC-encoded class I molecules. *Curr Opin Immunol*. 1999;11(1):100–8.

91. Tabiasco J, Rabot M, Aguerre-Girr M, El Costa H, Berrebi A, Parant O, et al. Human Decidual NK Cells: Unique Phenotype and Functional Properties – A Review. *Placenta*. 2006;27(SUPPL.):34–9.

92. Thielens A, Vivier E, Romagné F. NK cell MHC class I specific receptors (KIR): From biology to clinical intervention. *Curr Opin Immunol*. 2012;24(2):239–45.

93. Rizzo R. HLA-G molecules in pregnancy and their possible role in assisted reproductive technology. *Expert Rev Obstet Gynecol*. 2014;4(4):455–70.

94. Loustau M, Anna F, Dréan R, Lecomte M, Langlade-Demoyen P, Caumartin J. HLA-G Neo-Expression on Tumors. *Front Immunol*. 2020;11:1–15.

95. Negrini S, Contini P, Murdaca G, Puppo F. HLA-G in Allergy: Does It Play an Immunoregulatory Role? *Front Immunol*. 2021;12:1–8.

96. Baricordi O, Stignani M, Melchiorri L, Rizzo R. HLA-G and inflammatory diseases. *Inflamm Allergy Drug Targets*. 2008;7(2):67–74.

97. Ongaro A, Stignani M, Pellati A, Melchiorri L, Massari L, Caruso G, et al. Human leukocyte antigen-G molecules are constitutively expressed by synovial fibroblasts and upmodulated in osteoarthritis. *Hum Immunol*. 2010;71(4):342–50.

98. Lemaoult J, Zafaranloo K, Le Danff C, Carosella ED. HLA-G up-regulates ILT2, ILT3, ILT4, and KIR2DL4 in antigen presenting cells, NK cells, and T cells. *Fed Am Soc Exp Biol*. 2005;19(6):1–23.

99. Shiroishi M, Tsumoto K, Amano K, Shirakihara Y, Colonna M, Braud VM, et al. Human inhibitory receptors Ig-like transcript 2 (ILT2) and ILT4 compete with CD8 for MHC class I binding and bind preferentially to HLA-G. *Proc Natl Acad Sci U S A*. 2003;100(15):8856–61.

100. Contini P, Ghio M, Poggi A, Filaci G, Indiveri F, Ferrone S, et al. Soluble HLA-A,-B,-C and -G molecules induce apoptosis in T and NK CD8+ cells and inhibit cytotoxic T cell activity through CD8 ligation. *Eur J Immunol*. 2003;33(1):125–34.

101. LeMaoult J, Krawice-Radanne I, Dausset J, Carosella ED. HLA-G1-expressing antigen-presenting cells induce immunosuppressive CD4+ T cells. *Proc Natl Acad*

Sci U S A. 2004;101(18):7064–9.

102. Ristich V, Liang S, Zhang W, Wu J, Horuzsko A. Tolerization of dendritic cells by HLA-G. *Eur J Immunol*. 2005;35(4):1133–42.

103. Lila N, Rouas-Freiss N, Dausset J, Carpentier A, Carosella ED. Soluble HLA-G protein secreted by allo-specific CD4+ T cells suppresses the allo-proliferative response: A CD4+ T cell regulatory mechanism. *Proc Natl Acad Sci U S A*. 2001;98(21):12150–5.

104. Riteau B, Menier C, Khalil-Daher I, Sedlik C, Dausset J, Rouas-Freiss N, et al. HLA-G inhibits the allogeneic proliferative response. *J Reprod Immunol*. 1999;43(2):203–11.

105. Coupel S, Moreau A, Hamidou M, Horejsi V, Soulillou J-P, Charreau B. Expression and release of soluble HLA-E is an immunoregulatory feature of endothelial cell activation. *Blood*. 2007;109(7):2806–14.

106. Ulbrecht M, Honka T, Person S, Johnson JP, Weiss EH. The HLA-E gene encodes two differentially regulated transcripts and a cell surface protein. *J Immunol*. 1992;149(9):2945–53.

107. Sullivan LC, Clements CS, Rossjohn J, Brooks AG. The major histocompatibility complex class Ib molecule HLA-E at the interface between innate and adaptive immunity. *Tissue Antigens*. 2008;72(5):415–24.

108. Foroni I. HLA-E, HLA-F and HLA-G — The Non-Classical Side of the MHC Cluster. In: Couto AR, editor. HLA and Associated Important Diseases. Rijeka: IntechOpen; 2014. p. Ch. 3.

109. Joosten SA, Sullivan LC, Ottenhoff THM. Characteristics of HLA-E Restricted T-Cell Responses and Their Role in Infectious Diseases. *J Immunol Res*. 2016;2016:1–11.

110. Krangel MS. Two forms of HLA class I molecules in human plasma. *Hum Immunol*. 1987;20(2):155–65.

111. Krangel MS. Secretion of HLA-A and -B antigens via an alternative RNA splicing

pathway. *J Exp Med*. 1986;163(5):1173.

112. Calis JJA, Maybeno M, Greenbaum JA, Weiskopf D, De Silva AD, Sette A, et al. Properties of MHC Class I Presented Peptides That Enhance Immunogenicity. *PLoS Comput Biol*. 2013;9(10):e1003266.

113. Gallimore A, Dumrese T, Hengartner H, Zinkernagel RM, Rammensee H-G. Protective Immunity Does Not Correlate with the Hierarchy of Virus-specific Cytotoxic T Cell Responses to Naturally Processed Peptides. *J Exp Med*. 1998;187(10):1647-b.

114. Tenzer S, Wee E, Burgevin A, Stewart-Jones G, Friis L, Lamberth K, et al. Antigen processing influences HIV-specific cytotoxic T lymphocyte immunodominance. *Nat Immunol*. 2009;10(6):636–46.

115. Pang KC, Sanders MT, Monaco JJ, Doherty PC, Turner SJ, Chen W. Immunoproteasome Subunit Deficiencies Impact Differentially on Two Immunodominant Influenza Virus-Specific CD8+ T Cell Responses. *J Immunol*. 2006;177(11):7680–8.

116. Sette A, Vitiello A, Reherman B, Fowler P, Nayersina R, Kast WM, et al. The relationship between class I binding affinity and immunogenicity of potential cytotoxic T cell epitopes. *J Immunol*. 1994;153(12):5586–92.

117. Lazarski C, Chaves F, Jenks S, Wu S, Richards K. The kinetic stability of MHC class II: peptide complexes is a key parameter that dictates immunodominance. *Immunity*. 2005;23(1):29–40.

118. Chen W, Norbury C, Cho Y, Yewdell J. Immunoproteasomes Shape Immunodominance Hierarchies of Antiviral Cd8+ T Cells at the Levels of T Cell Repertoire and Presentation of Viral Antigens. *J Exp Med*. 2001;193(11):1319–26.

119. Crowe S, Turner S, Miller S, Roberts A-. Differential Antigen Presentation Regulates the Changing Patterns of CD8+ T Cell Immunodominance in Primary and Secondary Influenza Virus Infections. *J Exp Med*. 2003;198(3):399–410.

120. Gruta NL La, Kedzierska K, Pang K, Webby R, Davenport M, Chen W, et al. A virus-specific CD8+ T cell immunodominance hierarchy determined by antigen dose and

precursor frequencies. *Proc Natl Acad Sci U S A*. 2006;103(4):994–9.

121. Frankild S, de Boer RJ, Lund O, Nielsen M, Kesmir C. Amino acid similarity accounts for T cell cross-reactivity and for "holes" in the T cell repertoire. *PLoS One*. 2008;3(3):1–8.

122. Gebe J, Yue B, Unrath K, Falk B. Restricted autoantigen recognition associated with deletional and adaptive regulatory mechanisms. *J Immunol*. 2009;183(1):59–65.

123. Rolland M, Nickle DC, Deng W, Frahm N, Brander C, Learn GH, et al. Recognition of HIV-1 peptides by host CTL is related to HIV-1 similarity to human proteins. *PLoS One*. 2007;2(9):1–8.

124. Casp CB, She JX, McCormack WT. Genes of the LMP/TAP cluster are associated with the human autoimmune disease vitiligo. *Genes Immun*. 2003;4(7):492–9.

125. Handunnetthi L, Ramagopalan S V., Ebers GC, Knight JC. Regulation of MHC class II gene expression, genetic variation and disease. *Genes Immun*. 2010;11(2):99.

126. Kambayashi T, Laufer TM. Atypical MHC class II-expressing antigen-presenting cells: can anything replace a dendritic cell? *Nat Rev Immunol*. 2014;14(11):719–30.

127. Roche PA, Furuta K. The ins and outs of MHC class II-mediated antigen processing and presentation. *Nat Rev Immunol*. 2015;15(4):203–16.

128. Rock KL, Reits E, Neefjes J. Present Yourself! By MHC Class I and MHC Class II Molecules. *Trends Immunol*. 2016;37(11):724–37.

129. Rock KL, Gramm C, Rothstein L, Clark K, Stein R, Dick L, et al. Inhibitors of the proteasome block the degradation of most cell proteins and the generation of peptides presented on MHC class I molecules. *Cell*. 1994;78(5):761–71.

130. Michalek MT, Grant EP, Gramm C, Goldberg AL, Rock KL. A role for the ubiquitin-dependent proteolytic pathway in MHC class I-restricted antigen presentation. *Nature*. 1993;363(6429):552–4.

131. Reits E, Griekspoor A, Neijssen J, Groothuis T, Jalink K, Van Veelen P, et al. Peptide diffusion, protection, and degradation in nuclear and cytoplasmic compartments before antigen presentation by MHC class I. *Immunity*. 2003;18(1):97–108.

132. Neefjes J, Jongsma MLM, Paul P, Bakke O. Towards a systems understanding of MHC class I and MHC class II antigen presentation. *Nat Rev Immunol*. 2011;11(12):823–36.

133. Cresswell P, Bangia N, Dick T, Diedrich G. The nature of the MHC class I peptide loading complex. *Immunol Rev*. 1999;172:21–8.

134. Wearsch PA, Cresswell P. Selective loading of high-affinity peptides onto major histocompatibility complex class I molecules by the tapasin-ERp57 heterodimer. *Nat Immunol*. 2007;8(8):873–81.

135. Serwold T, Gonzalez F, Kim J, Jacob R, Shastri N. ERAAP customizes peptides for MHC class I molecules in the endoplasmic reticulum. *Nature*. 2002;419(6906):480–3.

136. Saric T, Chang SC, Hattori A, York IA, Markant S, Rock KL, et al. An IFN-gamma-induced aminopeptidase in the ER, ERAP1, trims precursors to MHC class I-presented peptides. *Nat Immunol*. 2002;3(12):1169–76.

137. Saveanu L, Carroll O, Lindo V, Del Val M, Lopez D, Lepelletier Y, et al. Concerted peptide trimming by human ERAP1 and ERAP2 aminopeptidase complexes in the endoplasmic reticulum. *Nat Immunol*. 2005;6(7):689–97.

138. Chang SC, Momburg F, Bhutani N, Goldberg AL. The ER aminopeptidase, ERAP1, trims precursors to lengths of MHC class I peptides by a “molecular ruler” mechanism. *Proc Natl Acad Sci U S A*. 2005;102(47):17107–12.

139. York IA, Chang SC, Saric T, Keys JA, Favreau JM, Goldberg AL, et al. The ER aminopeptidase ERAP1 enhances or limits antigen presentation by trimming epitopes to 8-9 residues. *Nat Immunol*. 2002;3(12):1177–84.

140. Nguyen TT, Chang SC, Evnouchidou I, York IA, Zikos C, Rock KL, et al. Structural basis for antigenic peptide precursor processing by the endoplasmic reticulum aminopeptidase ERAP1. *Nat Struct Mol Biol*. 2011;18(5):604–13.

141. Roelse J, Grommé M, Momburg F, Hämmerling G, Neefjes J. Trimming of TAP-translocated peptides in the endoplasmic reticulum and in the cytosol during recycling. *J Exp Med*. 1994;180(5):1591–7.

142. Alberts B, Johnson A, Lewis J, Raff M, Roberts K, Walter P. The Innate and Adaptive Immune Systems. In: Lanier L, editor. Molecular Biology of the Cell. 6th ed. Garland Science; 2015.

143. Osińska I, Popko K, Demkow U. Perforin: An important player in immune response. Central European Journal of Immunology. 2014.

144. Suri A, Lovitch SB, Unanue ER. The wide diversity and complexity of peptides bound to class II MHC molecules. *Curr Opin Immunol*. 2006;18(1):70–7.

145. Embgenbroich M, Burgdorf S. Current concepts of antigen cross-presentation. *Front Immunol*. 2018;9(JUL):1643.

146. Stern LJ, Brown JH, Jardetzky TS, Gorga JC, Urban RG, Strominger JL, et al. Crystal structure of the human class II MHC protein HLA-DR1 complexed with an influenza virus peptide. *Nature*. 1994;368(6468):215–21.

147. Cresswell P, Roche PA. Invariant chain–MHC class II complexes: always odd and never invariant. *Immunol Cell Biol*. 2014;92(6):471–2.

148. Neefjes J. CIIV, MIIC and other compartments for MHC class II loading. *Eur J Immunol*. 1999;29(5):1421–5.

149. Kleijmeer MJ, Morkowski S, Griffith JM, Rudensky AY, Geuze HJ. Major Histocompatibility Complex Class II Compartments in Human and Mouse B Lymphoblasts Represent Conventional Endocytic Compartments. *J Cell Biol*. 1997;139(3):639–49.

150. Denzin LK, Cresswell P. HLA-DM induces CLIP dissociation from MHC class II alpha beta dimers and facilitates peptide loading. *Cell*. 1995;82(1):155–65.

151. Boes M, Cerny J, Massol R, Op Den Brouw M, Kirchhausen T, Chen J, et al. T-cell engagement of dendritic cells rapidly rearranges MHC class II transport. *Nature*. 2002;418(6901):983–8.

152. Kleijmeer M, Ramm G, Schuurhuis D, Griffith J, Rescigno M, Ricciardi-Castagnoli P, et al. Reorganization of multivesicular bodies regulates MHC class II antigen presentation by dendritic cells. *J Cell Biol*. 2001;155(1):53–63.

153. Wubbolts R, Fernandez-Borja M, Oomen L, Verwoerd D, Janssen H, Calafat J, et al. Direct vesicular transport of MHC class II molecules from lysosomal structures to the cell surface. *J Cell Biol*. 1996;135(3):611–22.

154. Sansom DM, Manzotti CN, Zheng Y. What's the difference between CD80 and CD86? *Trends Immunol*. 2003;24(6):313–8.

155. Sheth S, Brito R, Mukherjea D, Rybak LP, Ramkumar V, Warrington R, et al. Cellular and Molecular Immunology. *Nat Rev Immunol*. 8th Editio. 2015;13(2):2–11.

156. Park J, Mazare A, Schneider H, Von Der Mark K, Fischer MJM, Schmuki P. Electric Field-Induced Osteogenic Differentiation on TiO2 Nanotubular Layer. *Tissue Eng - Part C Methods*. 2016;22(8):1–54.

157. LE B, S A, CE P. A pulsed current electric field alters protein expression creating a wound healing phenotype in human skin cells. *Regen Med*. 2020;15(5):1611–23.

158. Li K, Ning T, Wang H, Jiang Y, Zhang J, Ge Z. Nanosecond pulsed electric fields enhance mesenchymal stem cells differentiation via DNMT1-regulated OCT4/NANOG gene expression. *Stem Cell Res Ther*. 2020;11(1):1–14.

159. Zhao H, Steiger A, Nohner M, Ye H. Specific Intensity Direct Current (DC) Electric Field Improves Neural Stem Cell Migration and Enhances Differentiation towards βIII-Tubulin+ Neurons. *PLoS One*. 2015;10(6):1–21.

160. Kumar A, Nune K, Misra R. Understanding the response of pulsed electric field on osteoblast functions in three-dimensional mesh structures: *J Biomater Appl*. 2016;31(4):594–605.

161. TA B, PS L, JE F, JJ C-W. Effects of electric fields on human mesenchymal stem cell behaviour and morphology using a novel multichannel device. *Integr Biol (Camb)*. 2015;7(6):693–712.

162. Hakoda M, Hirota Y. Correlation between dielectric property by dielectrophoretic levitation and growth activity of cells exposed to electric field. *Bioprocess Biosyst Eng*. 2013;36(9):1219–27.

163. Zhao M, Bai H, Wang E, Forrester J V., McCaig CD. Electrical stimulation directly

induces pre-angiogenic responses in vascular endothelial cells by signaling through VEGF receptors. *J Cell Sci*. 2004;117(3):397–405.

164. Wang E, Zhao M, Forrester J V., MCCaig CD. Re-orientation and faster, directed migration of lens epithelial cells in a physiological electric field. *Exp Eye Res*. 2000;71(1):91–8.

165. Kumar A, Nune KC, Misra RDK. Electric field-mediated growth of osteoblasts-the significant impact of dynamic flow of medium. *Biomater Sci*. 2016;4(1):136–44.

166. Kolosnjaj-Tabi J, Gibot L, Fourquaux I, Golzio M, Rols MP. Electric field-responsive nanoparticles and electric fields: physical, chemical, biological mechanisms and therapeutic prospects. *Adv Drug Deliv Rev*. 2019;138:56–67.

167. Kirson ED, Dbalý V, Tovaryš F, Vymazal J, Soustiel JF, Itzhaki A, et al. Alternating electric fields arrest cell proliferation in animal tumor models and human brain tumors. *Proc Natl Acad Sci U S A*. 2007;104(24):10152.

168. Arruda-Neto JDT, Friedberg EC, Bittencourt-Oliveira MC, Cavalcante-Silva E, Schenberg ACG, Rodrigues TE, et al. Static electric fields interfere in the viability of cells exposed to ionising radiation. *Int J Radiat Biol*. 2009;85(4):314–21.

169. Tai G, Tai M, Zhao M. Electrically stimulated cell migration and its contribution to wound healing. *Burn Trauma*. 2018;6(20):1–7.

170. Yao L, Shanley L, Mccaig C, Zhao M. Small applied electric fields guide migration of hippocampal neurons. *J Cell Physiol*. 2008;216(2):527–35.

171. Oroza MA, Calcicedo L, Sanchez-Franco F, Rivas L. Hormonal, Hematological and Serum Chemistry Effects of Weak Pulsed Electromagnetic Fields on Rats. *Electromagn Biol Med*. 1987;6(2):139–51.

172. Stuchly MA, Ruddick J, Villeneuve D, Robinson K, Reed B, Lecuyer DW, et al. Teratological assessment of exposure to time-varying magnetic field. *Teratology*. 1988;38(5):461–6.

173. Zecca L, Dal Conte G, Furia G, Ferrario P. The effect of alternating magnetic fields on experimental inflammation in the rat. *Bioelectrochemistry Bioenerg*. 1985;14(1–

3):39–43.

174. Walleczek J. Electromagnetic field effects on cells of the immune system: the role of calcium signaling. *FASEB J*. 1992;6(13):3177–85.

175. Hoare JI, Rajnicek AM, McCaig CD, Barker RN, Wilson HM. Electric fields are novel determinants of human macrophage functions. *J Leukoc Biol*. 2016;99(6):1141–51.

176. Koga T, Morotomi-Yano K, Sakugawa T, Saitoh H, Yano K ichi. Nanosecond pulsed electric fields induce extracellular release of chromosomal DNA and histone citrullination in neutrophil-differentiated HL-60 cells. *Sci Rep*. 2019;9(1):1–13.

177. Rosado MM, Simkó M, Mattsson MO, Pioli C. Immune-Modulating Perspectives for Low Frequency Electromagnetic Fields in Innate Immunity. *Front Public Heal*. 2018;6:1–13.

178. Ohtani S, Ushiyama A, Maeda M, Ogasawara Y, Wang J, Kunugita N, et al. The effects of radio-frequency electromagnetic fields on T cell function during development. *J Radiat Res*. 2015;56(3):467–74.

179. Hilpert F, Heiser A, Wieckhorst W, Arnold N, Kabelitz D, Jonat W, et al. The impact of electrical charge on the viability and physiology of dendritic cells. *Scand J Immunol*. 2005;62(4):399–406.

180. Montgomery RA, Tatapudi VS, Leffell MS, Zachary AA. HLA in transplantation. *Nat Rev Nephrol 2018 149*. 2018;14(9):558–70.

181. Anonymous. Immunosuppressive drugs and their complications. *Drug Ther Bull*. 1994;32(9):66–70.

182. Sheikh AQ, Taghian T, Hemingway B, Cho H, Kogan AB, Narmoneva DA. Regulation of endothelial MAPK/ERK signalling and capillary morphogenesis by low-amplitude electric field. *J R Soc Interface*. 2013;10(78):1–13.

183. Greenbaum D, Colangelo C, Williams K, Gerstein M. Comparing protein abundance and mRNA expression levels on a genomic scale. *Genome Biol*. 2003;4(9):1–8.

184. Kendrick N. A gene's mRNA level does not usually predict its protein level. 2012. 1–

6 p.

185. Vogel C, Marcotte EM. Insights into the regulation of protein abundance from proteomic and transcriptomic analyses. *Nat Rev Genet*. 2012;13(4):227–32.

186. Cai X, Li P, Chen B, Li Q, Tang J, Zou X. Effect of high-voltage electrostatic field on cryopreservation of human epidermal melanocytes. In: E3S Web of Conferences. EDP Sciences; 2021. p. 1–4.

187. Hernández-Bule ML, Paíno CL, Trillo MÁ, Úbeda A. Electric stimulation at 448 kHz promotes proliferation of human mesenchymal stem cells. *Cell Physiol Biochem*. 2014;34(5):1741–55.

188. I B, DE D. Electric field induced changes in protein conformation. *Soft Matter*. 2014;10(3):431–7.

189. Titushkin I, Cho M. Regulation of Cell Cytoskeleton and Membrane Mechanics by Electric Field: Role of Linker Proteins. *Biophys J*. 2009;96(2):717–28.

190. Ray PD, Huang BW, Tsuji Y. Reactive oxygen species (ROS) homeostasis and redox regulation in cellular signaling. *Cell Signal*. 2012;24(5):981.

191. Andersen JK. Oxidative stress in neurodegeneration: cause or consequence? *Nat Med*. 2004;10 Suppl(7):18–25.

192. Shukla V, Mishra SK, Pant HC. Oxidative stress in neurodegeneration. *Adv Pharmacol Sci*. 2011;2011:1–12.

193. Trachootham D, Alexandre J, Huang P. Targeting cancer cells by ROS-mediated mechanisms: a radical therapeutic approach? *Nat Rev Drug Discov*. 2009;8(7):579–91.

194. Haigis MC, Yankner BA. The aging stress response. *Mol Cell*. 2010;40(2):333–44.

195. Zhang Y, Dong F, Liu Z, Guo J, Zhang J, Fang J. Nanosecond pulsed electric fields promoting the proliferation of porcine iliac endothelial cells: An in vitro study. *PLoS One*. 2018;13(5):1–12.

196. Minamitani Y, Kobayashi Y, Kageyama R. Investigation of difference of origin of

ROS generated in a cell by frequency components of pulsed electric field. *Dig Tech Pap Int Pulsed Power Conf*. 2015;2015-Octob:1–4.

197. Tanori M, Casciati A, Zambotti A, Pinto R, Gianlorenzi I, Pannicelli A, et al. Microsecond Pulsed Electric Fields: An Effective Way to Selectively Target and Radiosensitize Medulloblastoma Cancer Stem Cells. *Int J Radiat Oncol Biol Phys*. 2021;109(5):1495–507.

198. Khatib L, Golan DE, Cho M. Physiologic electrical stimulation provokes intracellular calcium increase mediated by phospholipase C activation in human osteoblasts. *FASEB J*. 2004;18(15):1903–5.

199. Bielfeldt M, Rebl H, Peters K, Sridharan K, Staehlke S, Nebe · J Barbara. Sensing of Physical Factors by Cells: Electric Field, Mechanical Forces, Physical Plasma and Light—Importance for Tissue Regeneration. *Biomed Mater Devices 2022*. 2022;1:1–16.

200. Cho MR, Thatte HS, Silvia MT, Golan DE. Transmembrane calcium influx induced by ac electric fields. *FASEB J*. 1999;13(6):677–83.